FINITE-ELEMENT MODELLING OF THE NEWBORN EAR CANAL AND MIDDLE EAR

Brian Gariepy

A thesis submitted to the Faculty of Graduate Studies and Research in partial fulfilment of the requirements of the degree of Master of Engineering

Department of Biomedical Engineering
McGill University
Montreal, Quebec
August 2010

ABSTRACT

Hearing loss is a very common birth defect. However, current hearing screening does not provide adequate specificity. Tympanometry is a potential hearing-screening tool that is specific to conductive hearing loss, but the tympanograms of newborns are currently not standardized and not well understood.

Finite-element models of the newborn ear canal and middle ear are developed and their responses to the tympanometric probe tone are studied. Low-frequency and dynamic simulations are used to model the ear's response to sound frequencies up to 2000 Hz. Material properties are taken from previous measurements and estimates, and the sensitivities of the models to these different parameters are examined. The simulation results are validated through comparison with previous experimental measures. Finally, the relative admittances of the ear canal and the middle ear at different frequencies are examined and implications for the interpretation of newborn tympanometry are discussed.

SOMMAIRE

La perte d'audition est une anomalie congénitale très courante. Toutefois, le dépistage auditif actuel n'est pas spécifique. La tympanométrie est un dépistage auditif potentiel qui aide à dépister la surdité de transmission, mais les tympanogrammes des nouveau-nés ne sont pas bien compris ou standardisés.

Deux modèles d'éléments finis ont été développés: l'un pour le conduit auditif des nouveau-nés, et l'autre pour l'oreille moyenne. Leurs réponses au ton de sonde tympanométrique sont étudiées. Les simulations quasi-statiques et dynamiques sont utilisés pour modeler la réponse de l'oreille aux fréquences de son jusqu'à 2000 Hz. Les propriétés matérielles sont prises des mesures et des estimations précédentes, et les sensibilités des modèles à ces différents paramètres sont examinées. Les résultats des simulations sont validés par la comparaison avec les mesures expérimentales précédentes. Enfin, les impédances relatives du canal externe de l'oreille et de l'oreille moyenne aux fréquences différentes sont examinées et les implications pour l'interprétation de la tympanométrie du nouveau-né sont discutées.

ACKNOWLEDGEMENTS

I would like to thank my supervisors, Dr W Robert J Funnell and Dr Sam J Daniel for their guidance and for the inspiration for this project. My frequent meetings with Dr Funnell were especially useful for keeping my work on track and discussing the next step in the research.

I would also like to thank all of my colleagues in the lab for their suggestions and the help they provided with any problems I had, and my family and friends for their support and encouragement. Also, I would like to especially thank Dr. Li Qi for granting me access to his models and data.

This work was funded by the Canadian Institutes of Health Research and the Natural Sciences & Engineering Research Council (Canada).

TABLE OF CONTENTS

LIST OF FIGURES

CHAPTER 1: INTRODUCTION

1.1 MOTIVATION

It is estimated that approximately 6 out of every 1000 newborns are born with some hearing deficiency (Marazita *et al.*, 1993). However, this estimate includes cases where the hearing loss is transient and benign, predominantly caused by an accumulation of amniotic fluid and mesenchyme in the ear canal and middle-ear cavity. This fluid will typically drain from the ear within a few days after birth and the child will have no developmental delays.

The first few years of a child's life are the most important for language development. The presence of a slight hearing deficiency may be enough to inhibit a child's learning and may result in speech and behavioural problems (NIDCD, 1993; ASHA, 1994). Therefore, an accurate test of a newborn's hearing capacity is needed, demonstrated by the fact that newborn hearing screening is mandated in several provinces and states.

Currently, there are two popular newborn hearing tests being used by hospitals in North America: auditory brain-stem response (ABR) and otoacoustic emissions (OAE). ABR measures the electrical activity of the auditory neurons in response to acoustic stimulation of the ear, while OAE measures the amplitude of the evoked sounds emitted by the outer hair cells of the cochlea. Although both of these tests are efficient at detecting the presence of hearing loss, neither of them can reliably give insight into the nature of the problem. For example, neither test is able to reliably determine whether a detected hearing loss is conductive or sensorineural. (Conductive hearing loss is defined as hearing loss caused by outer and/or middle-ear problems, and sensorineural hearing loss is defined as hearing loss caused by inner-ear and/or auditory-nerve problems.) Due to the importance of correctly identifying the type of detected hearing loss, particularly in

regard to treatment options, these tests are not sufficient and a different category of hearing test is required.

Tympanometry is a test that measures the input admittance of the ear canal and middle ear. (Admittance is defined in Section 2.8.1.) The measurement is performed by introducing a small-amplitude probe tone into the ear canal in the presence of a static pressure. This test is sensitive only to conductive hearing problems and could therefore add specificity to a diagnosis obtained with ABR or OAE. However, the results of this test in newborns are currently not well understood. It is quite common for a tympanogram taken from a newborn with perfect hearing to be diagnosed as pathological, as well for a tympanogram measured from a newborn with known middle-ear problems to be diagnosed as being normal (e.g., Paradise *et al.* 1976, Meyer *et al* 1997, Watters *et al.* 1997). Consequently, it is obvious that the ears of newborns and adults react differently to the tympanometric input, suggesting that a better understanding of the mechanics of the newborn ear canal and middle ear is required before the results of this test can be used with confidence.

Directly studying the mechanics of the newborn ear, although desirable, is difficult. It would be imperative that these investigations be done on children under the age of 1 month due to the major changes to ear structure that occur as the child ages. It would therefore be very difficult to acquire data and to determine the underlying causes of the measured behaviour. Finite-element modelling (FEM) is a useful way to study newborn ear mechanics. With FEM, assuming the use of relatively accurate geometry, boundary conditions and material properties, fairly realistic simulations of tympanometric tests on the newborn ear can be performed. After validation with whatever experimental data are available, FEM simulations can be used to study the effects of anatomical differences, pathological conditions, etc. Furthermore, FEM provides access to data that would unobtainable through experimental means, such as the sensitivity of the system to variations of certain physical parameters as well as precise, simultaneous displacement measurements at every point in the geometry.

As mentioned above, the tympanometric input signal is composed of two major parts: a large-amplitude static pressure and a low-amplitude probe tone. Previous work has already been done on the response of a FE model of the newborn ear canal and middle ear to large static pressures (Qi *et al.* 2006, 2008). However, there has been no work done on the response of this FE model to the probe tone. In order to obtain a better understanding of the differences between adult and newborn tympanometry, this research will analyze the behaviour of FE models of the newborn ear canal and middle ear in response to the tympanometric probe tone.

1.2 OUTLINE

The thesis will continue with a brief review of the relevant anatomy and of the basic principles of tympanometry in Chapter 2. Then, in Chapter 3, the different methods that are used in this research, such as the finite-element method, Rayleigh damping, and the Elementary Effects Method will be discussed. A detailed description of the finite-element models of the newborn ear canal and middle ear will be presented in Chapter 4. That chapter will also include the reasoning behind the choices of the material properties and boundary conditions in the two types of simulations that are run: low-frequency simulations and dynamic simulations. Chapter 5 will present the results that are obtained from these simulations, and then Chapter 6 will present the conclusions and the potential for future work.

CHAPTER 2: ANATOMY AND TYMPANOMETRY

2.1 INTRODUCTION

This chapter will review the anatomy of the human ear. First, a quick overview of the ear as a whole and a list of its major components will be given. This will be followed by a much more detailed description of these components and their roles in the function of the ear. Also, the basic principles of tympanometry in both adults and newborns will be discussed.

2.2 OVERVIEW OF EAR ANATOMY

The human ear is commonly broken down into three major sections: the outer ear, the middle ear, and the inner ear, as seen in Figure 2.1. The visible part of the outer ear is known as the pinna or auricle. Its main purpose is to funnel sound energy from the environment into the ear canal. At the medial end of the ear canal is the tympanic membrane (TM), which is considered to be the first structure of the middle ear. It is a very thin structure that vibrates when stimulated by incoming sound energy from the canal. There are three ossicles that are attached in series to the TM: the malleus, incus and stapes. When the TM vibrates, it causes these bones to vibrate, leading to the transfer of energy from the footplate of the stapes to the liquid behind the oval window of the cochlea (the first structure of the inner ear). The volume of air that lies between the TM and the cochlea and houses the three ossicles is known as the middle-ear cavity. The cavity is connected directly to the nasal cavity through the Eustachian tube. The cochlea is a liquid-filled, spiralling structure that contains four rows of hair cells that extend along the length of the spiral. When the fluid in the cochlea is stimulated by the stapes, it causes these hairs to bend, leading to the firing of action potentials in the auditory nerve. This signal is transmitted through a series of nerves and nuclei to the auditory cortex and is perceived as sound.

The role of the middle ear in hearing is impedance matching and sound transmission. If the middle ear were not present, most of the air-borne sound energy would be reflected rather than transmitted into the cochlea due to the much larger impedance of the cochlear fluid relative to air. Although the situation is not really so simple (Funnell 1996), the middle ear can be thought of as matching these two impedances by means of three mechanisms: the relative surface areas of the TM and the stapes footplate; the lever ratio of the ossicles; and the curvature of the TM.

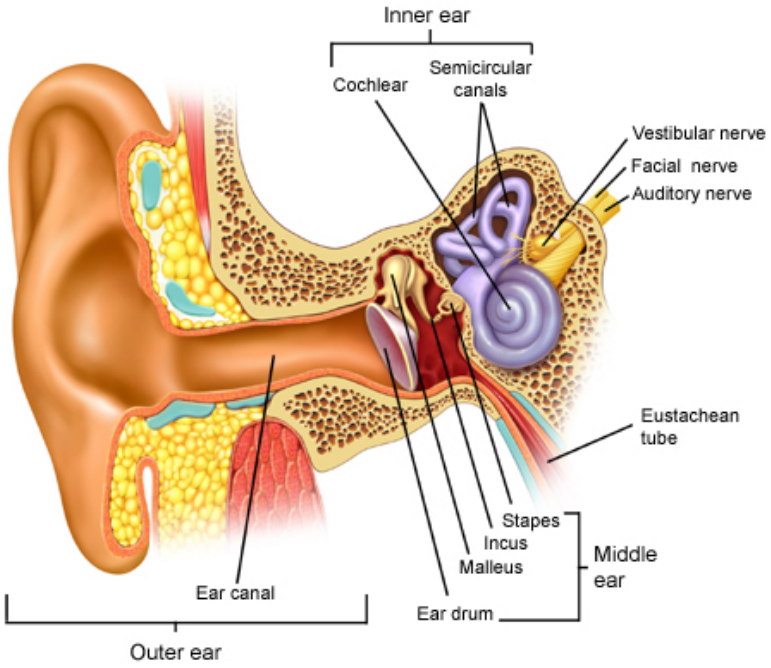

Figure 2.1 Human ear anatomy (Source: http://www.virtualmedicalcentre.com as of 25 August 2010)

2.3 PINNA

Despite its seemingly simple purpose, the pinna is a complex anatomical structure containing several different components, such as the helix, antihelix, tragus, antitragus, concha and lobule. Each of these structures is comprised mainly of cartilage. The pinna collects sound energy and directs it into the ear canal (e.g., Widmaier *et al.* 2006). The pinna typically grows at the same rate as the head and neck during a child's development until the child is approximately 6 − 9 years of age. At this point the pinna has reached its adult size (Anson and Donaldson, 1981).

2.4 EAR CANAL

The ear canal is the second structure of the outer ear. It transmits sound energy towards the middle ear. It produces a substance known as cerumen (ear wax) in order to protect the canal walls from infection.

For the purposes of this research, the most interesting aspects of the ear-canal anatomy are not its final, adult structure, but rather the changes that take place in the ear canal after birth. Unlike most structures of the middle and inner ear, the auditory canal has not reached its adult size at birth and will undergo significant changes during a child's first few years of life. A summary of these changes can be seen in Figure 2.2.

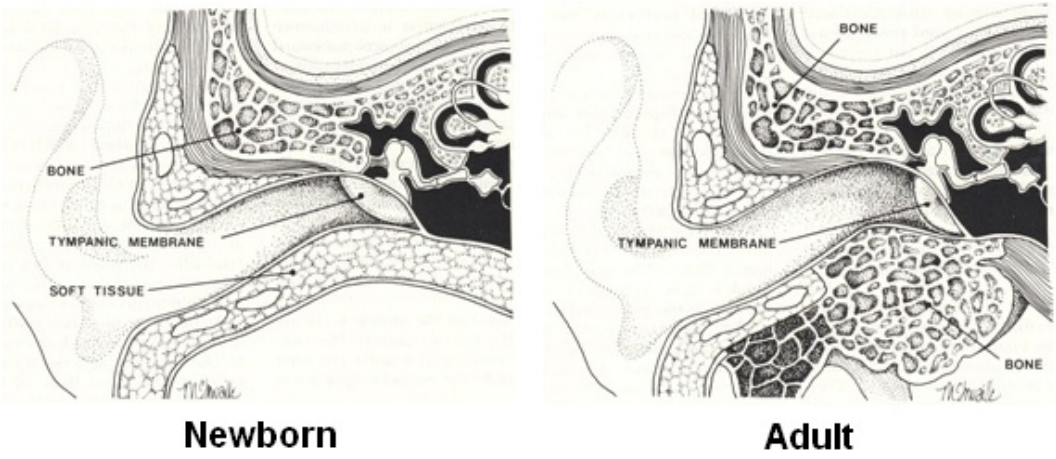

Figure 2.2 Comparison of newborn and adult ear canals. Modified from Bluestone (1983)

Two major differences between the ear canal of the newborn and that of the adult are the shape and size. The newborn canal is relatively straight and is considerably shorter and narrower than its adult counterpart. The length of the newborn canal ranges from 13 to 22.5 mm and the average diameter of the canal is approximately 4.44 mm (McLellan and Webb 1957; Keefe *et al.* 1993). By contrast, in the adult the ear canal is not straight; it typically contains two major turns (not shown in Figure 2.2) and is therefore normally described as having an "S shape". The canal grows considerably with age. Adult canals have a length of approximately 30 mm and a diameter of approximately 10 mm (Saunders *et al.* 1983; Stinson and Lawton 1989).

Another functionally important change that occurs in the development of the canal is in its composition. In the newborn, the canal wall is surrounded along most of its length by elastic cartilage (McLellan and Webb 1957), the most flexible type of cartilage in the human body (Fung *et al.* 1993). This causes the newborn canal to be very compliant. Once the child reaches approximately four months of age, bone has grown around much of the canal. In the adult, only the most lateral third of the canal wall is composed of elastic cartilage, while the medial two-thirds of the canal are encompassed by temporal bone (Keefe and Levi 1996).

2.5 TYMPANIC MEMBRANE

The tympanic membrane (TM), or eardrum, is a thin, multi-layered structure that is considered to be the boundary between the outer and middle ear. It is functionally broken down into two different sections: the pars flaccida and the pars tensa. In humans, the pars flaccida is the smaller of the two components and is located superior to the manubrium (the part of the malleus that connects directly to the TM). Though its role is not really known, it has been suggested that it may have a role in detecting the presence of small, static middle-ear pressures due to its outstanding pressure sensitivity (Didyk *et al.* 2007).

The pars tensa, the larger of the two TM components as seen in Figure 2.3, consists of three different layers. The outer layer is an epidermal layer resembling the skin found elsewhere on the body; the intermediate layer contains mainly fibrous elements; and the innermost layer is a mucosal layer. In humans, the pars tensa constitutes the vast majority of the TM's surface area and is primarily responsible for the transfer of energy from the canal to the ossicles. The TM is described as having a conical shape with the umbo (at the tip of the manubrium) as the deepest point. It is encompassed by the fibrocartilaginous ring which firmly connects the edge of the TM to the tympanic ring of the temporal bone.

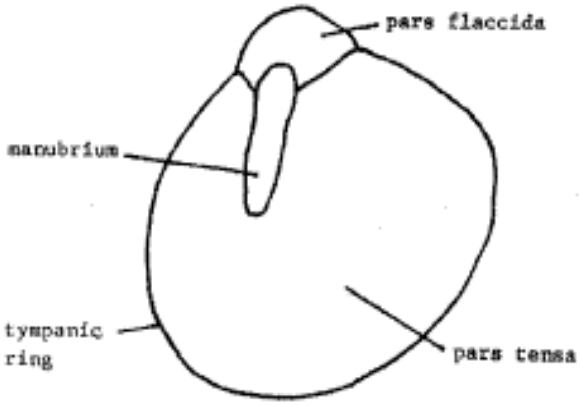

Figure 2.3 Anatomy of the human TM. From Ladak (1993), after Kojo (1954)

Despite the fact that the human TM remains the same size throughout life (Anson and Donaldson 1981), there are distinct morphological differences between the TM of a newborn and that of an adult. These changes include cellularity, vascularity, and orientation within the skull. The TM of the adult is positioned much more vertically than is that of the newborn. However, the difference that may be of greatest significance for the purpose of this research is the thickness of the membrane. Confocal microscopy measurements of adult TMs show that the majority of its surface has a relatively constant thickness in the range of 0.04 to 0.12 mm (Kuypers *et al.* 2006). The TM of the newborn, however, has been shown to be generally thicker with a much higher degree of non-uniformity (Ruah *et al.* 1991). A more detailed description of this distinction and its impact on the modelling process will be given in Chapter 4.

2.6 OSSICLES

The three ossicles of the middle ear are the malleus, incus and stapes, which can be seen in Figure 2.4.

The malleus is connected to the tip of the TM's conical form through a long region known as the manubrium. The head of the malleus is attached to the body of the incus via the incudomallear joint, and the incus in turn is connected to the stapes through the incudostapedial joint (between the lenticular process of the incus and the head of the stapes). Between the long process of the incus and the lenticular process is an extremely thin and flexible region of bone known as the pedicle which is thought to have a large role in the mechanics of the middle ear (Funnell *et al.* 2005). The malleus is attached to the temporal bone by superior, lateral and anterior ligaments while the incus is attached to the bone by posterior and superior ligaments. However, the only two ligaments that are modelled in this research are the anterior mallear ligament (AML) and the posterior incudal ligament (PIL). The ossicular chain also contains a pair of antagonist muscles known as the tensor tympani muscle and the stapedius muscle.

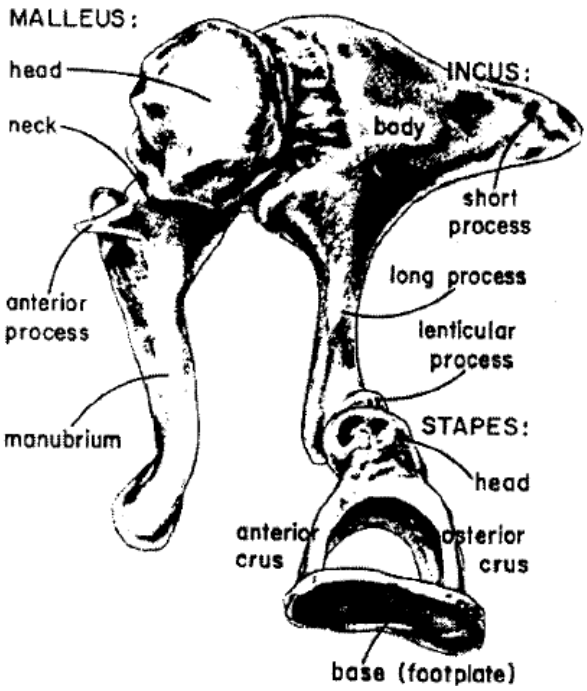

Figure 2.4 Anatomy of the human ossicles. From Donaldson et al (1992).

2.7 MIDDLE-EAR CAVITY AND EUSTACHIAN TUBE

The middle-ear cavity is an air-filled space located on the medial side of the TM; it is bounded by the temporal bone and contains the ossicles. It is connected to the nasal cavity through the Eustachian tube. However, this tube is usually in a closed state. The size of the middle-ear cavity in the human adult is highly variable among individuals, ranging between 2 and 22 cc (Molvaer *et al.* 1978). It is said that the volume of the middle-ear cavity changes quite dramatically as a newborn ages, though there have been no detailed measurements made of the dimensions of the newborn's cavity.

The Eustachian tube has a couple of very important functions in hearing. First, any secretions produced inside the middle ear will collect at the bottom of the cavity and will be transferred to the nasal cavity via the Eustachian tube. This prevents an accumulation of fluid behind the TM that would interfere with TM vibrations and that could potentially lead to infection. Its second function is to maintain a balance in static pressure between the two sides of the TM. Since the TM is securely attached to the tympanic ring, there is a seal formed between the middle-ear cavity and the external air. In order to avoid a large accumulation of static pressure on the TM, the Eustachian tube can open temporarily (usually during yawning or swallowing) to allow for this pressure to be periodically rebalanced. This is crucial since a build-up of pressure in the cavity will lead to altered hearing as well as discomfort.

2.8 TYMPANOMETRY

2.8.1 GENERAL DESCRIPTION

Tympanometry is a clinical test that measures the immitance at the TM under a variety of different static pressures. Immitance is discussed in detail below. The tympanometer itself is a relatively simple device that is mildly invasive in the sense that it requires a small probe to be inserted partway into the ear canal. It is extremely important for the precision and validity of the results that the probe tip forms a hermetic seal with the walls of the ear canal.

The tympanometer contains four major components: a microphone, an air pump, a manometer and a loudspeaker. This configuration can be seen in Figure 2.5. The air pump is used to adjust the static pressure inside the ear canal so that the immitance can be measured over a range of static pressures. In one approach, once the static pressure has been set, a single-frequency probe tone is generated by the loudspeaker and is kept at a predetermined sound pressure level using feedback generated by the microphone. The amount of feedback necessary to maintain a constant probe-tone sound pressure can be converted to an equivalent immitance value.

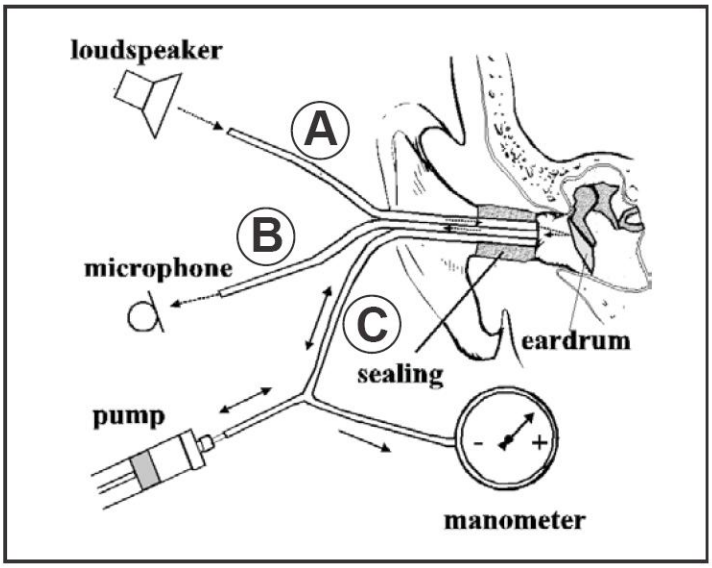

Figure 2.5 Diagram including the primary components of a tympanometer. From Qi (2008)

Immitance describes the relationship between an input sound pressure and the resulting volume velocity of a mechanical body. The volume velocity of a surface is defined as the integral over that surface of the component of particle velocity normal to the surface. (In the case of a simple piston, for example, the volume velocity of its face is the piston velocity multiplied by its surface area.) Immitance itself is a generic term that includes two reciprocal quantities: admittance (Y) and impedance (Z). The respective equations for these quantities are:

$$Y = \frac{U}{P} \tag{2.1}$$

and

$$Z = \frac{P}{U} \tag{2.2}$$

where P is the input sound pressure and U is the volume velocity. Both of these representations of the immitance are used in the current literature, and the remainder of this report will utilize both terms. Immitance is a complex quantity since it involves both the magnitude and the phase of the pressure/velocity relationship. In the case of admittance, the real component is known as the conductance (G) while the imaginary component is known as the susceptance (B). For the impedance, the real and imaginary terms are known as the resistance (R) and the reactance (X) respectively.

For any mechanical or acoustical system, there are three different classes of parameters that control the dynamic force-displacement relationship: damping, mass, and stiffness. These three parameters are directly related to the complex immitance. Conductance and resistance are measurements of friction and energy dissipation and would therefore be determined by the damping parameters. Since in a passive system energy can only be dissipated and not created, the real part of the immitance cannot take a negative value and the phase angle is subsequently bound between −90 and +90 degrees. Conversely, the susceptance and reactance are measures of the energy storage of the system and would therefore be determined by the net effect of the mass and

stiffness terms. These imaginary components will generally be positive at low frequencies (indicative of a stiffness-dominated system), negative at high frequencies (indicative of a mass-dominated system), and zero at a resonance where the mass and stiffness terms are balanced.

Although the immitance measured by tympanometry corresponds to the signal generated by the canal walls, the air in the canal, and the middle ear, it is almost always only the latter measurement that is of interest. Therefore, a method is needed to isolate the middle-ear immitance from the immitance generated by the other two sources. As mentioned in the anatomy description, the majority of the adult canal is encased by temporal bone. This greatly limits the movement of the walls, and for this reason the immitance of the canal wall is considered to be negligible when compared with that of the middle ear and is therefore ignored. The immitance of the enclosed air, however, is of larger magnitude and cannot be ignored. Therefore, during clinical tympanometry, an immitance reading in the presence of a large static pressure (either positive or negative) is performed. This large pressure will push the TM and the middle ear to their limits and cause the structures to become essentially rigid. Therefore, in this situation, the immitance measurement will isolate the effect of the air in the canal, and this admittance can be subtracted from the unpressurized admittance measurement to give the admittance of the middle ear alone.

Although any acoustic frequency could be used for the probe tone, the most common choice for clinical purposes is 226 Hz. This frequency is chosen for two major reasons. The first is that it is far enough below the resonance frequency of the middle ear (usually situated at approximately 1000 Hz) that the mass and damping terms are negligible, allowing for the measured results to be interpreted as pure stiffness. The second reason is that by using this frequency when calculating the canal-air admittance, 1 mmho of admittance ('mho' is the inverse of 'ohm', and 1 mmho = 10 $mm^3/s/Pa$) corresponds to exactly 1 cc of air (Katz *et al.* 2002), allowing for an easy determination of total ear-canal volume. However, it has been shown that pathologies such as middle-

ear effusion can be detected more efficiently when using higher probe-tone frequencies (e.g. Shurin *et al.* 1977, Marchant *et al.* 1984, Hunter and Margolis, 1992).

During a clinical tympanogram, the static pressure is typically varied between −400 and +200 daPa (1 daPa = 10 Pa) and the admittance is measured in both the right and left ear. A healthy ear will display a relatively large peak in admittance near 0 dB of static pressure, implying that the TM vibration amplitude is large. However, abnormalities can present themselves in the form of a shifted peak, an unusually large or small peak, an unusually large or small ear-canal volume, etc. A list and some visual examples of different types of tympanogram abnormalities and the pathologies behind them can be seen in Table 2.1 and Figure 2.6.

Type	Characteristics	Indication
A	Peaks at 0 daPa	Normal
Ad:	Unusually high peak	Suggests ossicular dislocation.
As:	Reduced peak	Suggests ossicular fixation.
B:	Flat, no peak	Indicates reduced movement, usually a sign of middle ear fluid or a space-occupying tumor.
Type B with an abnormally large volume	>2.0 cc volume	Indicates a perforation or patent ventilation tube.
Type C:	Negative pressure	Indicates abnormal negative peak.
Type D: Notching	Shows a dip in the peak	Indicates scarred eardrums or a hypermobile tympanic membrane (TM).
Type B with an abnormally small ear canal volume	< 1.0 cc	Indicates faulty probe function, usually the probe is against the ear canal wall or blocked with cerumen.

Table 2.1 A description of the different low-frequency adult tympanometric diagnoses. From Jerger (1970), after Linden (1969)

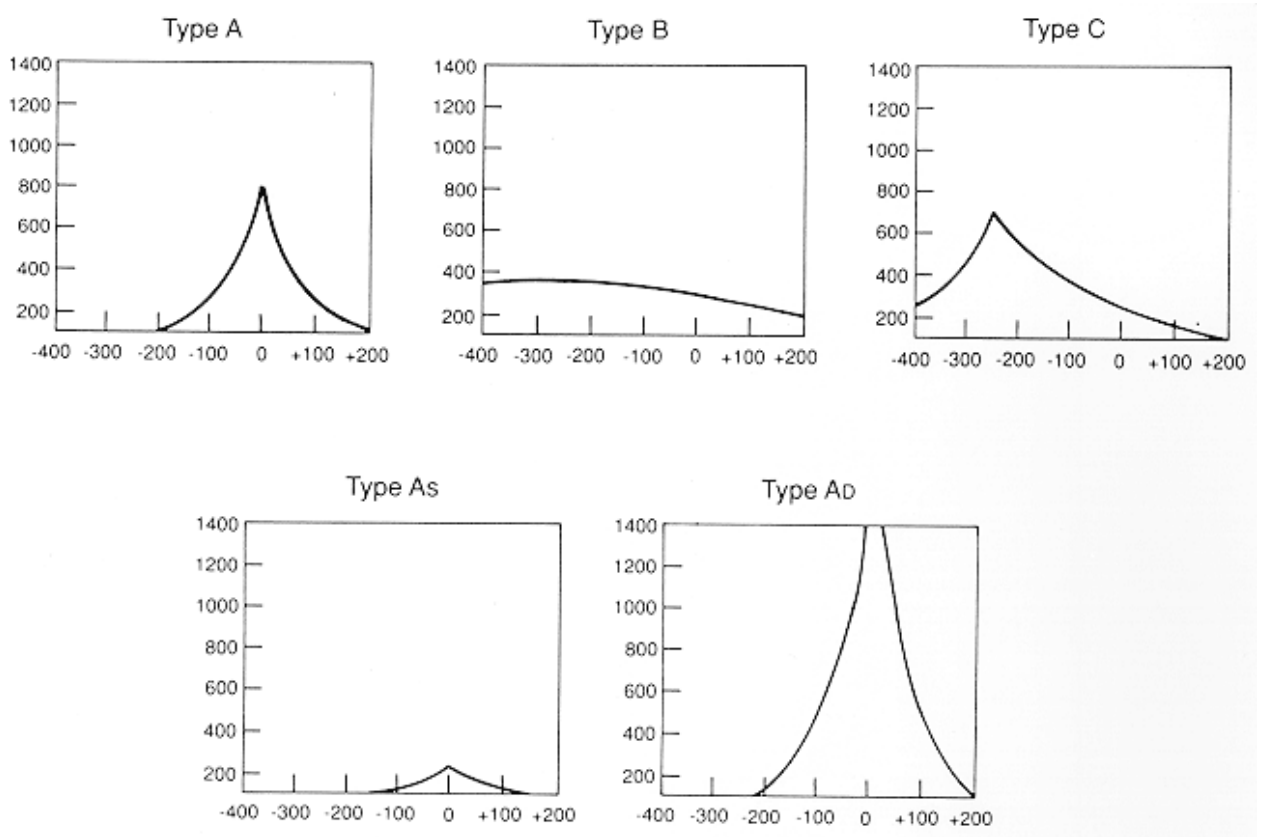

Figure 2.6 A visual representation of some of the different types of tympanograms discussed in Table 2.1. X and Y axes are pressure and admittance respectively. (Source: http://www.ivertigo.net)

2.8.2 NEWBORN TYMPANOMETRY

As mentioned in Section 1.1, newborn tympanometry results are currently not well understood, and the results obtained when using a 226 Hz probe tone do not relate well to the state of the child's middle ear. For example, even though the infant tympanograms in Figure 2.7 correspond to normal hearing in the right ear and middle-ear effusion in the left ear, the 226-Hz tympanograms give very similar results in both ears. Recent research has suggested that more informative and reliable results can be obtained using higher-frequency probe tones when testing newborns, more specifically, probe tones of approximately 1000 Hz (e.g., Margolis and Popelka, 1975; Margolis *et al.* 2003; Alaerts *et al.* 2007). Although the exact reason for these improved results are not known, it is thought that they are due to developmental changes in the size of the ear structures, the orientation of the TM, the fusing of the tympanic ring to the temporal bone, a decrease in the mass of the middle ear, the ossification of the canal wall, etc. (Holte *et al.* 1991). It is likely that multi-frequency tympanograms would provide the most meaningful results. However, due to the amount of time currently required for this type of examination, it is thought to be impractical for hearing screening.

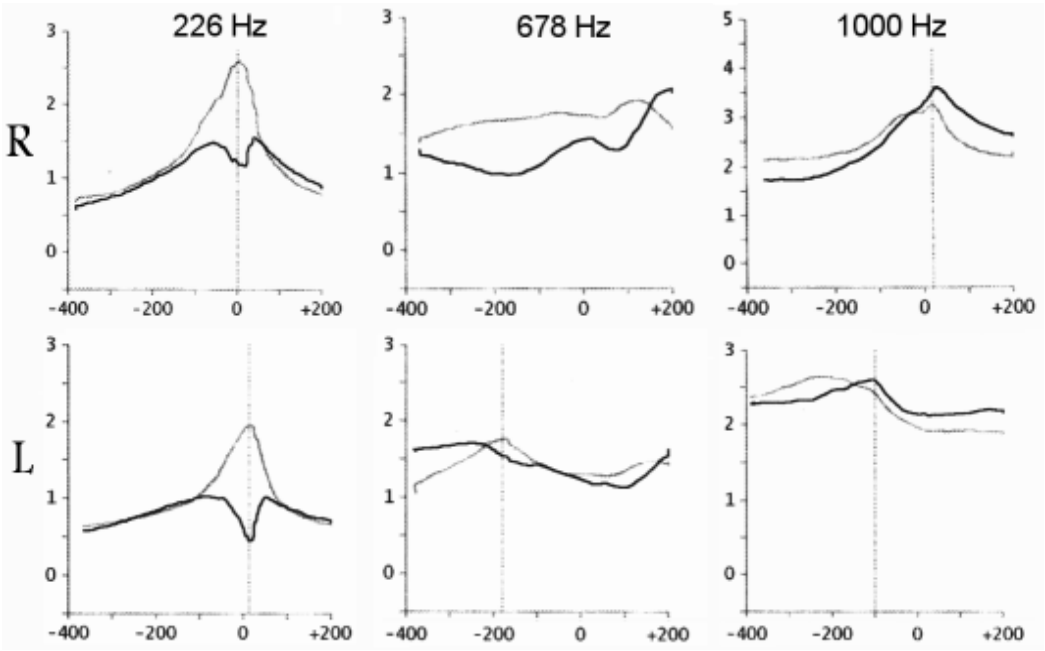

Figure 2.7 Clinical infant tympanogram. Dark lines are susceptance, light lines are conductance. Units for X and Y axes are daPa and mmho respectively. R and L signify the right and left ears.

CHAPTER 3: METHODS

3.1 INTRODUCTION

This chapter will include brief descriptions of the methods that are used in this research, including the finite-element method, Rayleigh damping, and the elementary-effects method. It will also include details regarding the construction of the model geometries and their meshes.

3.2 FINITE-ELEMENT METHOD

The finite-element method (FEM) will be used to calculate the response of a 3D model of the newborn ear canal and middle ear to sound pressures. The basic approach of FEM is to segment a large, complicated geometry into a finite number of simple elements. For solid models, triangular and tetrahedral elements are often chosen due to their computational simplicity and their ability to represent the geometry of any solid structure. All of these elements will share at least 2 corners (or *nodes*) with other elements in the structure.

The advantage of performing this segmentation is that an individual element has a much more simple and well-defined force-displacement relationship than the overall structure of which it forms part. For a structural mechanics problem, the differential equation for a single-degree-of-freedom system is

$$m\frac{d^2u}{dt^2} + c\frac{du}{dt} + ku = f(t) \tag{3.1}$$

where m is mass, c is damping, k is stiffness, u is displacement, and f is external force. This equation could be solved analytically in the case of a single degree of freedom, but for a large, irregularly shaped geometry, it would be difficult or impossible to derive an

analytic solution. It is for this reason that the geometry is instead broken down into small elements so that an approximate numerical solution can be determined. Each element will have multiple degrees of freedom (3 or 6 per node) and so Equation 3.1 must be converted to matrix form:

$$\mathbf{M}_e\ddot{\mathbf{u}} + \mathbf{C}_e\dot{\mathbf{u}} + \mathbf{K}_e\mathbf{u} = \mathbf{f}(t) \tag{3.2}$$

where $\mathbf{M}_e$, $\mathbf{C}_e$, and $\mathbf{K}_e$ are the mass, damping, and stiffness matrices of the element *e***.** A system matrix equation can then be generated to numerically solve for the overall system force-displacement relationship:

$$\mathbf{M}\ddot{\mathbf{u}} + \mathbf{C}\dot{\mathbf{u}} + \mathbf{K}\mathbf{u} = \mathbf{f}(t) \tag{3.3}$$

where **M**, **C**, and **K** are the mass, damping, and stiffness matrices of the full system**.** The basic principle is that if two of these elements share a common edge or face, then their individual force-displacement matrices can be combined to give the total relationship for the joined shape. An example of this can be seen in Figure 3.1 where triangles 1-2-3 and 2-3-4 share the common edge 2-3. Assuming a static simulation where only the stiffness term is present, the force (**f***,* **g**) and displacement (**w**) vectors for each of these triangles when isolated are related by their respective 3×3 stiffness matrices (**A**, **B**). When these triangles are joined, the 4×4 stiffness matrix for the newly formed quadrilateral is just a linear superposition of matrices **A** and **B**. By continuing this logic, any 3D surface can be created iteratively by adding additional triangles to the mesh, and the stiffness matrix will be updated in each iteration via simple linear superposition. This same logic can be applied to the mass and damping matrices as well when dealing with dynamic simulations. Further details on the finite-element method and the derivation of the stiffness, damping, and mass matrices can be found elsewhere (e.g., Hartley *et al.* 1986).

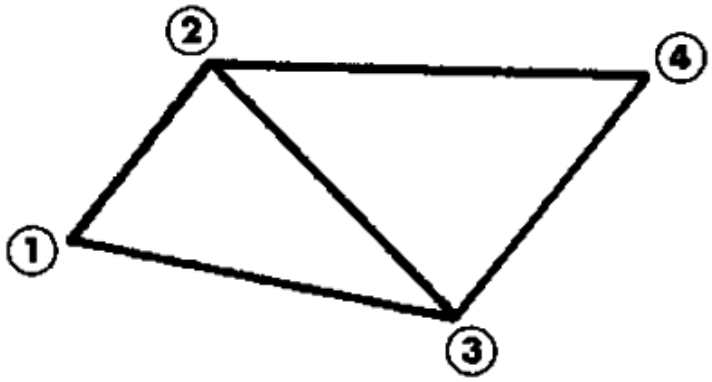

$$\begin{bmatrix} a_{11} & a_{12} & a_{13} \\ a_{21} & a_{22} & a_{23} \\ a_{31} & a_{32} & a_{33} \end{bmatrix} \begin{bmatrix} w_1 \\ w_2 \\ w_3 \end{bmatrix} = \begin{bmatrix} f_1 \\ f_2 \\ f_3 \end{bmatrix} \quad \text{and} \quad \begin{bmatrix} b_{11} & b_{12} & b_{13} \\ b_{21} & b_{22} & b_{23} \\ b_{31} & b_{32} & b_{33} \end{bmatrix} \begin{bmatrix} w_2 \\ w_3 \\ w_4 \end{bmatrix} = \begin{bmatrix} g_2 \\ g_3 \\ g_4 \end{bmatrix}$$

$$\begin{bmatrix} a_{11} & a_{12} & a_{13} & 0 \\ a_{21} & a_{22}+b_{11} & a_{23}+b_{12} & b_{13} \\ a_{31} & a_{32}+b_{21} & a_{33}+b_{22} & b_{23} \\ 0 & b_{31} & b_{32} & b_{33} \end{bmatrix} \begin{bmatrix} w_1 \\ w_2 \\ w_3 \\ w_4 \end{bmatrix} = \begin{bmatrix} f_1 \\ f_2+g_2 \\ f_3+g_3 \\ g_4 \end{bmatrix}$$

Figure 3.1 Basic example of system matrix construction in FEM. (Source: http://audilab.bme.mcgill.ca)

3.3 RAYLEIGH DAMPING

The damping of a mechanical system is more difficult to understand than its mass or stiffness since it deals with its internal friction and energy dissipation, processes that are difficult to isolate and measure. Therefore, several different models have been proposed for describing damping in a mechanical system. One of the more common models for damping, and the one that is used throughout this research, is Rayleigh damping. In this model, it is assumed that the damping matrix of Equation 3.3 is simply a linear combination of the mass and stiffness matrices:

$$\mathbf{C} = \alpha\mathbf{M} + \beta\mathbf{K} \tag{3.4}$$

where α and β are the mass and stiffness damping parameters. Although this formulation allows for the damping to be parameterized in a model, these two damping parameters don't have any physical significance and cannot be measured through experiments. In order to estimate the value of these parameters for a specific system, these parameters they are linked to a much more well-known and physically relevant parameter;, the damping ratio (ξ), which is defined as the ratio between an oscillator's actual damping and critical damping (e.g., Alciatore *et al*, 2007). The relationship between the Rayleigh damping parameters and the damping ratio is

$$\xi = \frac{1}{2}\left(\frac{\alpha}{\omega} + \beta\omega\right) \tag{3.5}$$

where ω is the angular input frequency (radians/sec). In order to solve for the two Rayleigh damping parameters, the damping ratio must be specified at two different angular frequencies:

$$\frac{1}{2}\begin{bmatrix} \frac{1}{\omega_1} & \omega_1 \\ \frac{1}{\omega_2} & \omega_2 \end{bmatrix}\begin{bmatrix} \alpha \\ \beta \end{bmatrix} = \begin{bmatrix} \xi_1 \\ \xi_2 \end{bmatrix} \tag{3.6}$$

Using this model of damping, it is impossible to obtain a system where the damping ratio is constant for all frequencies. As can be seen in Figure 3.2, if the damping ratio is chosen to be equal at two frequencies, then its value will be larger outside of this range and smaller in between.

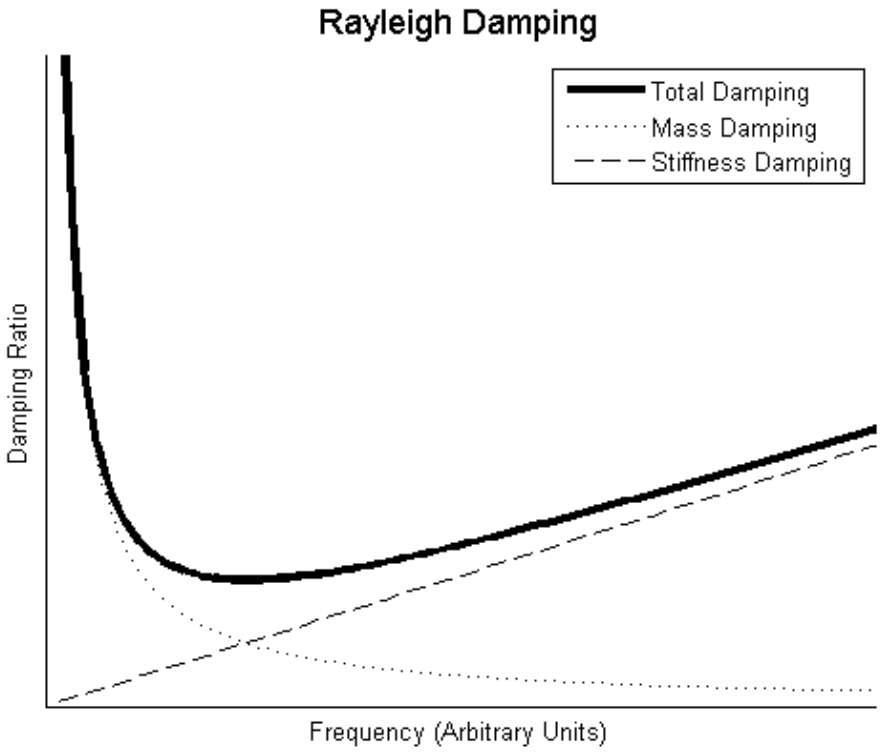

Figure 3.2 The dependence of the damping ratio on frequency in Rayleigh damping. The total damping is the sum of the mass and stiffness damping.

3.4 ELEMENTARY-EFFECTS METHOD

When running simulations on a large finite-element model with an abundance of parameters, it is useful to perform a sensitivity analysis on the system to determine the relative importance of the various parameters to the model output. This type of analysis can lead to an improved understanding of the system and help establish how much the uncertainty in the parameters can affect the output. This second benefit is particularly important in this work on the newborn ear due to the lack of knowledge about the magnitudes of parameters such as the Young's modulus of the TM. Sensitivity analysis will characterize the importance of the parameter estimates.

There are two major categories of sensitivity analysis: global and local. In global sensitivity analysis, the behaviour of the model is studied throughout a very large parameter space. This examination will result in an extremely thorough quantitative

description of how a model behaves for any combination of input parameters. However, for the purposes of this research, global sensitivity analysis is not necessary. Obtaining quantitative results is usually only necessary when the model will be repeatedly verified and updated, a procedure which will not be carried out in this study. Also, utilizing a very large parameter space is not effective when using a model that must contain physiologically meaningful values. Therefore, local sensitivity analysis will instead be used in this research. Local sensitivity analysis begins with the model situated at a certain base point in the parameter space and then describes the model's response to relatively small perturbations in the parameter set. These methods are most often carried out by changing one parameter at a time.

Perhaps the most commonly used local sensitivity analysis method for mechanical and acoustical models is the elementary-effects method (EEM) (Saltelli *et al.* 2004). The primary reasons for its popularity are its ability to describe nonlinear effects and interactions alongside overall parameter importance, and the fact that it does not rely on restrictive assumptions and is hence model independent. In EEM, the model is expressed in the form

$$Y = f(X_1, X_2, \ldots, X_k) \tag{3.7}$$

where Y is the output of interest and X_1 through X_k are normalized versions of the k input parameters. The range of each parameter is normalized to the range [0, 1] and divided into p levels, resulting in a region of experimentation that is a k-dimension p-level grid with the following possible parameter values:

$$X_i = \{0, \Delta, \ldots, 1 - \Delta, 1\} \tag{3.8}$$

where Δ is $1/(p-1)$. In this research, p is chosen to be 5 in order to have enough steps to provide a complete sensitivity description without requiring excessive computations. Within this region of experimentation, the elementary effect of input parameter i is simply the partial differential of the output with respect to that parameter:

$$d_i = \frac{Y(X_1, X_2, \ldots, X_i + \Delta, \ldots, X_k) - Y(X_1, X_2, \ldots, X_k)}{\Delta} \tag{3.9}$$

With this formula in mind, the parameter set is progressively moved through the region of experimentation by changing only one parameter at a time by the step size Δ, allowing for d_i to be calculated at every step. Once multiple (r) elementary effects have been calculated for every parameter (the effect of one parameter may change depending on the sampled point in the parameter space), then the sensitivity of parameter i can be described using the following two values:

$$\mu_i = \frac{1}{r} \sum_{j=1}^{r} d_i(X^{(j)}) \tag{3.10}$$

$$\sigma_i = \sqrt{\frac{1}{(r-1)} \sum_{j=1}^{r} (d_i(X^{(j)}) - \mu_i)^2} \tag{3.11}$$

where $X^{(j)}$ is the j-th set of input parameters (X_1, …, X_k). In this research, r is chosen to be 3 as this allows for the effect of each parameter to be measured as it moves between the upper limit, lower limit and centre of its range. The measure μ_i is a general measure of the importance of a certain parameter to the model output. Essentially, it is the average partial differential of the output with respect to that parameter over several different points in the region of experimentation. The measure σ_i describes the non-linear behaviour of that parameter and how it interacts with the other parameters of the system; it is calculated as the standard deviation of the parameter's partial differential. If a certain parameter has a large σ_i, then its importance is highly dependent on the value of the other parameters in the model. The exact procedures used for calculating the elementary effects of the model parameters are presented in Table A.1 and A.2.

3.5 GEOMETRY AND MESH GENERATION

Mesh generation is a crucial step in the finite-element modelling process since the accuracy and precision of the model solution is highly dependent on the quality of the mesh. In this research, several different programs are used to generate an accurate newborn ear geometry and the appropriate corresponding mesh. *Fie* is a program that is used to create the outline of the structure of interest. As an input, *Fie* takes a sequence of cross-sectional images at different slices depths. In each of these images, the program is used to draw lines along the borders of the regions of interest. For example, in the ear, these different regions would include the soft tissue, temporal bone, TM, ossicles etc. An example of a segmentation done using *Fie* is shown in Figure 3.3. Once this segmentation in complete for all slices, the lines are passed into a program named *Tr3* that connects all of the two-dimensional outlines of a subset together with triangles, allowing for a three-dimensional object to be formed from this series of two-dimensional images. These triangular surface meshes are converted to tetrahedral volume meshes using *Gmsh* (http://www.geuz.org/gmsh/), and the results of this conversion can be displayed in *Fad*. This final program can be used to check the integrity of the volume meshes and ensure that there are no overlaps or gaps present, and then it is used to join several different subset meshes together to get the overall mesh for the system to be studied. (*Fie, Tr3,* and *Fad* are all locally developed programs that can be found at http://audilab.bme.mcgill.ca/sw/.) The finalized mesh is imported into COMSOL™ version 3.2 (http://www.comsol.com) for finite-element analysis. Once the mesh is in COMSOL, the material properties and boundary conditions of the subsets must be specified before simulations can be run.

a)

b)

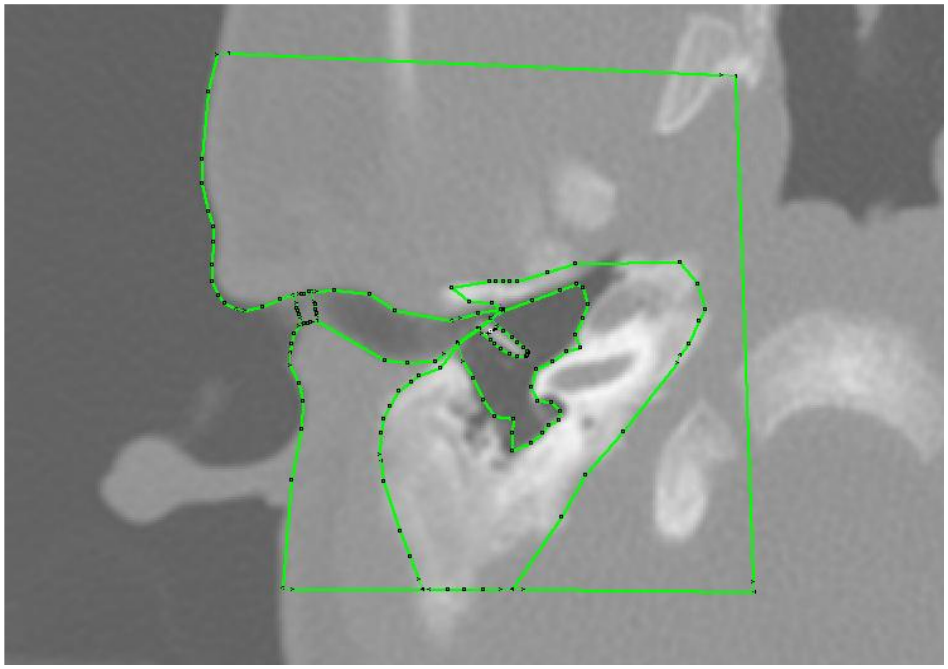

Figure 3.3 Examples of the CT scan slices and outlines used for model construction. a) Slice including outline of temporal bone. b) Slice including outlines of bone, ear canal, TM, malleus, probe tip and middle-ear cavity.

As the resolution of a finite-element mesh is increased and the model is divided into a larger number of smaller elements, the solved displacements should increase, monotonically or not, and should asymptotically approach the true values as shown in Figure 3.4. As the number of elements increases, the computational expense can increase dramatically. An important step in any finite-element analysis is the testing of different mesh resolutions to determine a resolution that is sufficiently fine but not too computationally expensive.

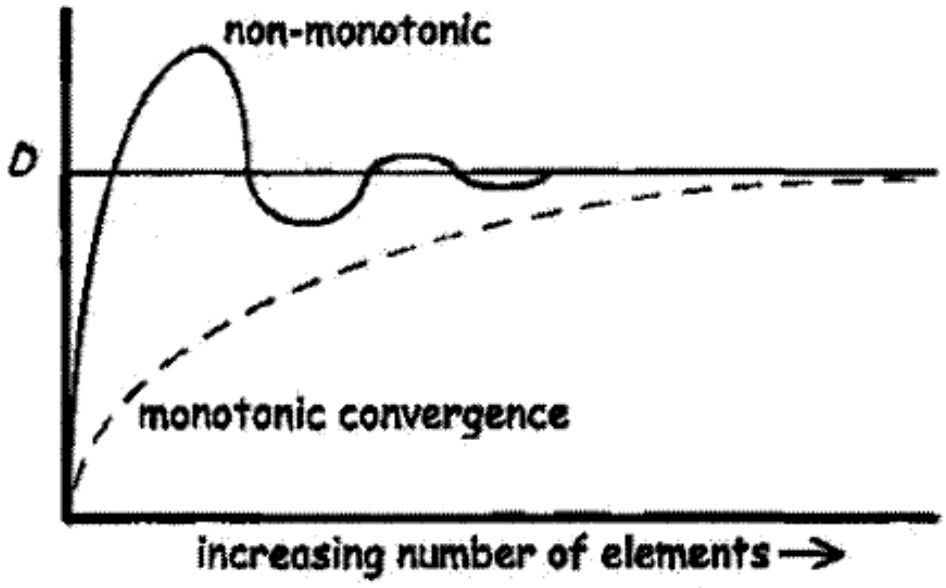

Figure 3.4 The difference between non-monotonic and monotonic convergence. D is the theoretical exact solution. From Siah (2002).

CHAPTER 4: FINITE-ELEMENT MODELS

4.1 INTRODUCTION

In this chapter, the process of building the geometry of the ear-canal and middle-ear models is described. This is followed by a description of the two different types of simulations that will be used in this research: low-frequency simulations and dynamic simulations. The boundary conditions and material properties for both of these simulation types are also presented.

4.2 MODEL GEOMETRY

The finite-element representation of the newborn ear was based on a series of cross-sectional images that were imported into *Fie* for segmentation. For this research, a clinical X-ray CT scan (GE LightSpeed16, Montreal Children's Hospital) of a 22-day-old newborn's right ear was used. Although this child was born with a unilateral congenital defect of the ear canal on the left side, the right ear was found to have no anatomical abnormalities and to exhibit normal hearing (Qi *et al*. 2006). The scan contains 47 different horizontal slices in the superior-inferior direction with a slice thickness of 0.625 mm. A large number of the slices do not show the ear canal or middle ear, but rather contain just soft tissue and cranial bones. (After this thesis had been written, examined and passed, and while minor modifications were being made, it was discovered that although the slice thickness of the CT scan is 0.625 mm, the slice spacing is actually 0.5 mm. Therefore, the model geometries in this thesis are elongated by 25% in the inferior-superior direction. Some implications of this error are discussed in Section 6.2.2.)

This same CT scan was segmented previously by Qi, a past graduate student in this lab, when he was studying the non-linear response of the newborn ear canal and middle ear to large static pressures (Qi *et al.* 2006, 2008). In order for the results of this

work to be consistent and possibly later combined with his, the same segmentation will be used in this study with only a few minor changes. When he did the segmentation, he separately outlined the structures of the canal and middle ear and studied them independently of one another. In this work, the simultaneous admittance of the canal and middle ear will be compared and therefore it is beneficial to have both of these systems combined into one model. In order to make these two systems compatible in the same model, the segmentation data were combined into one file and slight changes were made to some of the lines and their properties in order to achieve a fully compatible mesh (see Section 3.5). The resulting full model can be seen in Figure 4.1. Although the probe tip is obviously not present in the original CT scan, it is represented in the model by a small block located 5 mm inside of the ear canal (Keefe *et al.* 1993) and tightly connected with the surrounding tissue in order to simulate a hermetic seal.

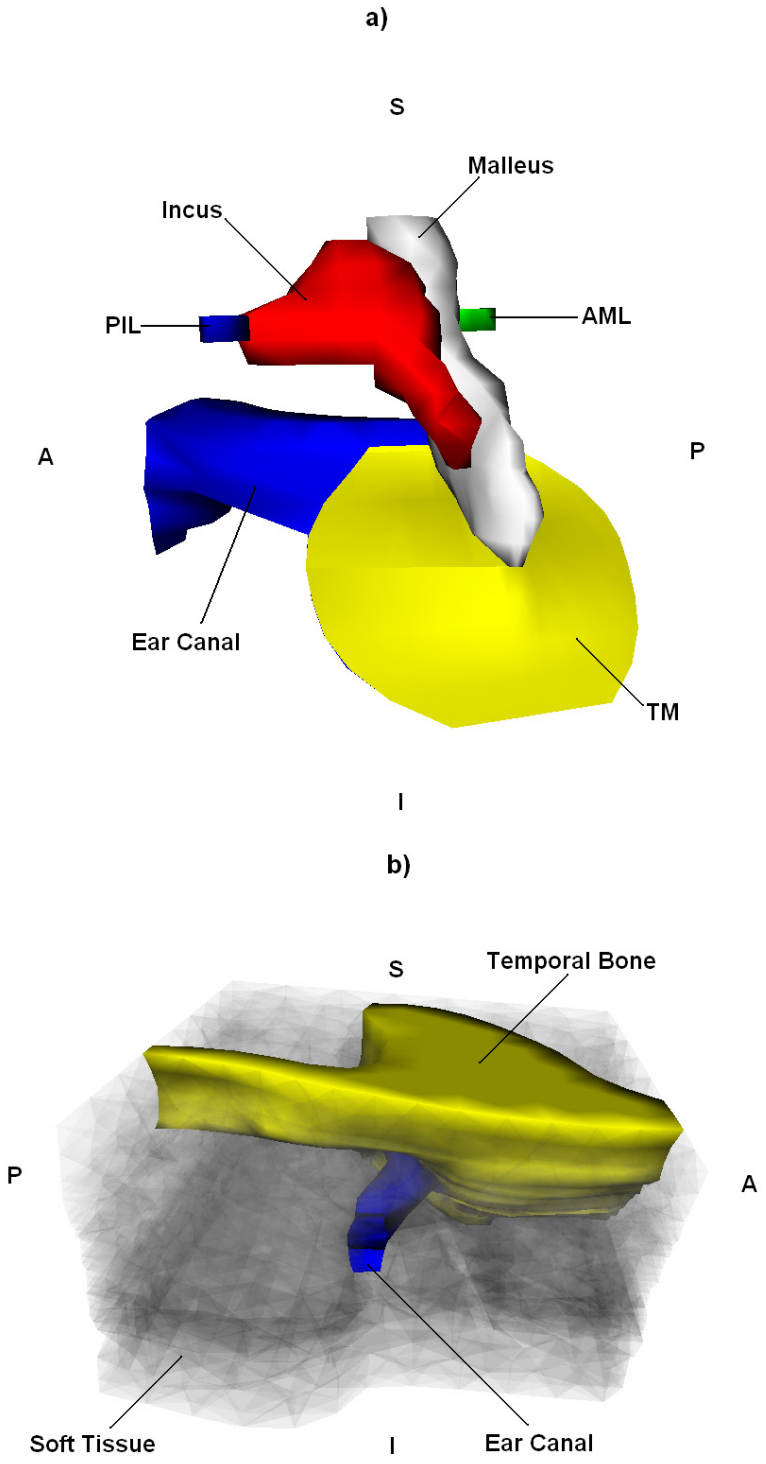

Figure 4.1 Complete model geometries. a) Medial view of the ear canal and middle ear. b) Lateral View of the ear canal, temporal bone and (partially transparent) soft tissue. S is superior, I is inferior, L is lateral, M is medial, A is anterior, P is posterior

4.3 BOUNDARY CONDITIONS

One of the major assumptions that will be made in this study is that the border of the TM is clamped in place around its periphery. In models of adult ears, human or otherwise, this assumption is often used (e.g., Funnell 1996, Ghosh *et al.* 1996, Siah 2002) since the TM is attached to the relatively very thick fibrocartilaginous ring, which in turn is securely attached to the tympanic ring of the temporal bone; in adults the tympanic ring is bone and it is immobile with respect to the head. In newborns, however, this assumption may not be as well-founded due to the fact that the tympanic ring is not fully developed and ossified until the child is two years old (Saunders *et al.* 1983). For this reason, the boundary of the newborn TM may not be completely clamped, but the extent of this possible movement has not yet been measured. The primary reason for including this assumption in the model is that it allows for the middle-ear simulations to be performed independently of the ear-canal simulations. The only interface between the ear canal and the middle ear in the model ear is the tympanic ring. If the ring is clamped, then any displacement of the ear canal will have no effect on the middle ear and vice versa, and the simulations of these two systems can be run separately, greatly reducing computation time and increasing efficiency.

Along with the tympanic ring and the ends of the AML and the PIL, the other structures that will be clamped during these simulations are the temporal bone, due to it being the primary reference point for all displacements in the model, and the probe tip since it is assumed to be securely fixed in place inside the ear canal. For the ear-canal simulations, the TM will be entirely clamped as it is only the wall displacements that are included in this case; the TM displacements will be analyzed in the middle-ear model. For low-frequency sound input, the wavelength of the sound pressure will be significantly longer than the ear canal itself, implying that the pressure will be of very similar magnitude throughout the canal. Therefore, the pressure in the simulations will be uniform everywhere inside the ear canal, and also across the TM in the middle-ear model. This assumption will be discussed in more detail in Section 4.5.3.

4.4 LOW-FREQUENCY SIMULATIONS

4.4.1 INTRODUCTION

As a first step in studying the response of the newborn middle ear and ear canal to the tympanometric probe tone, it is assumed that the probe-tone frequency is very low, or more specifically that it is far below the resonance frequency of both systems involved. This allows for simplifications to be made in the simulation process and for preliminary results to be obtained regarding the nature of the newborn ear. The overall goal of this section of the research is to use FEM to analyze the relative magnitudes of the admittance produced by the newborn's ear-canal wall and by the middle ear during tympanometry, and to compare the ratio to that seen in adults.

Normally when studying probe-tone stimulation, a harmonic input would be needed to imitate the sound wave pressure. However, the primary advantage of assuming a low-frequency probe tone is that the same results can be obtained using static inputs. The basic logic behind this simplification is that if the input frequency is low enough, the system has plenty of time to adjust to the changes in the pressure. This eliminates all of the transient behaviour that would normally be seen in a dynamic simulation, and the model displacements at any point in time would be dependent only on the input pressure at that time and not on what happened in the past. Therefore, static simulations at a constant input pressure level will be used for this initial work.

4.4.2 MATERIAL PROPERTIES

4.4.2.1 OVERVIEW

When looking at material properties, the first distinction that must be made is whether or not the materials are linear. In studying the response of these models to large static pressures, Qi *et al.* (2006, 2008) could not assume that the materials were linear and instead used a hyperelastic non-linear model. That material model assumes that a material

behaves linearly up to a certain strain, such as approximately 5%, before becoming stiffer (e.g., Holzapfel *et al.* 2000), as seen in Figure 4.2. Due to the fact that static pressures in tympanometry can reach up to 4000 Pa, there will certainly be large deformations in the ear and this change in stiffness will play a large role. In fact, Qi's results indicate that the onset of the stiffness non-linearity seems to occur at approximately 1000 Pa in both the ear canal and the middle ear (2008). The probe tone, however, is of much smaller amplitude than the static pressures (usually less than 1 Pa) and will certainly not cause a large enough deformation of the tissues to push the system into its non-linear range. Therefore, in all of the simulations of this research, all of the materials are assumed to be linear in order to increase the computational efficiency.

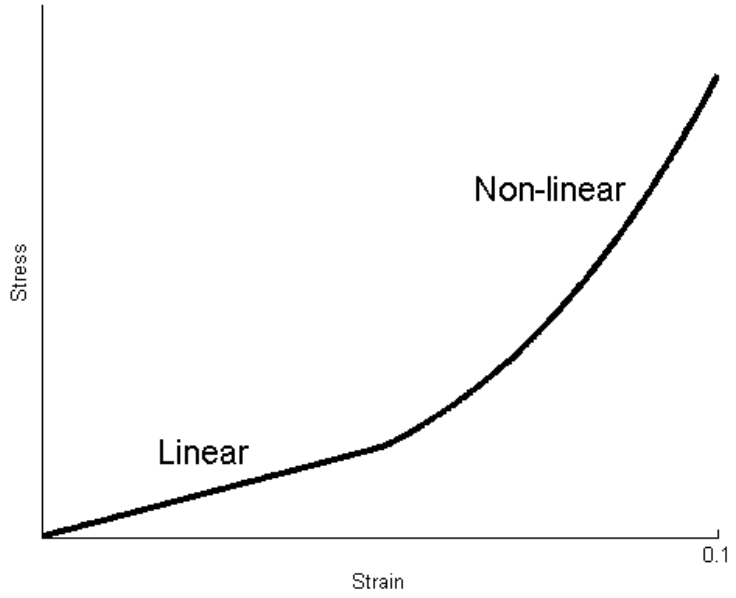

Figure 4.2 Stress-strain curve for hyperelastic materials.

Typically, the three major categories of material properties that need to be defined for a model are mass, damping and stiffness. However, as stated above, this initial work will only be using static simulations and thereby ignoring any time-dependent effects. Subsequently, as evidenced by Equation 3.3, all of the velocity and acceleration terms will be ignored, causing the mass and damping parameters of the materials to become irrelevant. Therefore, the only parameters that will play a role in these simulations are the

stiffnesses and Poisson's ratios of the tissues. In Qi's work, the Poisson's ratio was set at a value of 0.475 as this is a widely used value in the literature for modelling biological tissues (e.g. Cheung *et al.* 2004, Chui *et al.* 2004). Having the Poisson's ratio set at this value assumes that the tissue is nearly incompressible. (An incompressible material has a value of 0.5.) Qi *et al.* (2006) found that these types of ear models are largely insensitive to this parameter, and it is therefore assumed that setting the Poisson's ratio of the tissues to 0.475 will produce accurate behaviour.

4.4.2.2 SOFT TISSUE AND TYMPANIC MEMBRANE

Due to the linear nature of the materials in this work, the stiffness can be defined by a simple constant known as the Young's modulus: the ratio between the stress and the strain of a material. However, to this date, the Young's moduli of the newborn TM and ear-canal soft tissue have not been measured and are not known. The soft tissue that surrounds the ear canal in humans is elastic cartilage (McLellan and Webb, 1957), a tissue that has a Young's modulus in the range of 100kPa to 1MPa in adults (Zhang *et al.* 1997, Liu *et al.* 2004). However, the mechanical properties of this tissue change drastically in the early stages of life. It has been shown that the modulus of bovine cartilage increases by approximately 100% from foetus to newborn (Klein *et al.* 2007) and by another 275% from newborn to adult (Williamson *et al.* 2001).

For the TM, adult Young's modulus values have been measured in several different studies, and the resulting magnitudes lie in the range of 20-40 MPa (Békésy *et al.* 1960, Kirkae *et al.* 1960, Decraemer *et al.* 1980, Cheng *et al.* 2007). Similar to the case for the canal wall, there is likely to be a drastic change that occurs during development, and it has been estimated that the Young's modulus of a newborn's TM is approximately 7-8 times smaller than that of the adult (Qi *et al.* 2008). Since precise values for the Young's moduli of a newborn's elastic cartilage and TM are not available, a range of plausible values must be used instead.

For both of these modulus values, the ranges to be used will be based on those used by Qi *et al.* (2006, 2008). For the elastic cartilage surrounding the ear canal, he used a range of 30 kPa to 90 kPa. The lower boundary of this range coincides with the stiffness of some of the least stiff tissues of the human body, such as fat (Wellman *et al.* 1999), whereas the upper boundary coincides with the stiffness of the most compliant cartilage seen in adults. Although this range is wide, it almost certainly includes the true value of this parameter. Likewise for the modulus of the TM, the chosen range of values lies between 0.6 MPa and 2.4 MPa and is based on the information presented in the previous paragraph. The size of these ranges is likely the limiting factor for the precision of these models.

4.4.2.3 EFFECT OF FREQUENCY

The modulus values in the previous paragraph were used by Qi *et al.* to model a static input pressure. However, these values may need modification when attempting to model the response to a dynamic probe tone. Due to the viscoelastic nature of soft tissue, the elastic modulus will not be constant across all frequencies as demonstrated in Figure 4.3. At low frequencies, the modulus remains constant at its static value, but at a certain critical frequency, the modulus rises sharply before settling at a new high-frequency value. The critical frequency (ω_c) is defined as follows (Fung *et al.* 1993):

$$\omega_c = \frac{1}{\sqrt{\tau_\sigma \tau_\varepsilon}} \tag{4.1}$$

where τ_σ and τ_ε are the creep time and stress-relaxation time respectively. Assuming that these two processes can each be defined by the same individual time constant, the critical frequency simply becomes the reciprocal of the creep time. Therefore, an estimation of the creep time of these tissues is needed in order to calculate the value of this critical frequency and to determine if any adjustments are needed for the modulus ranges.

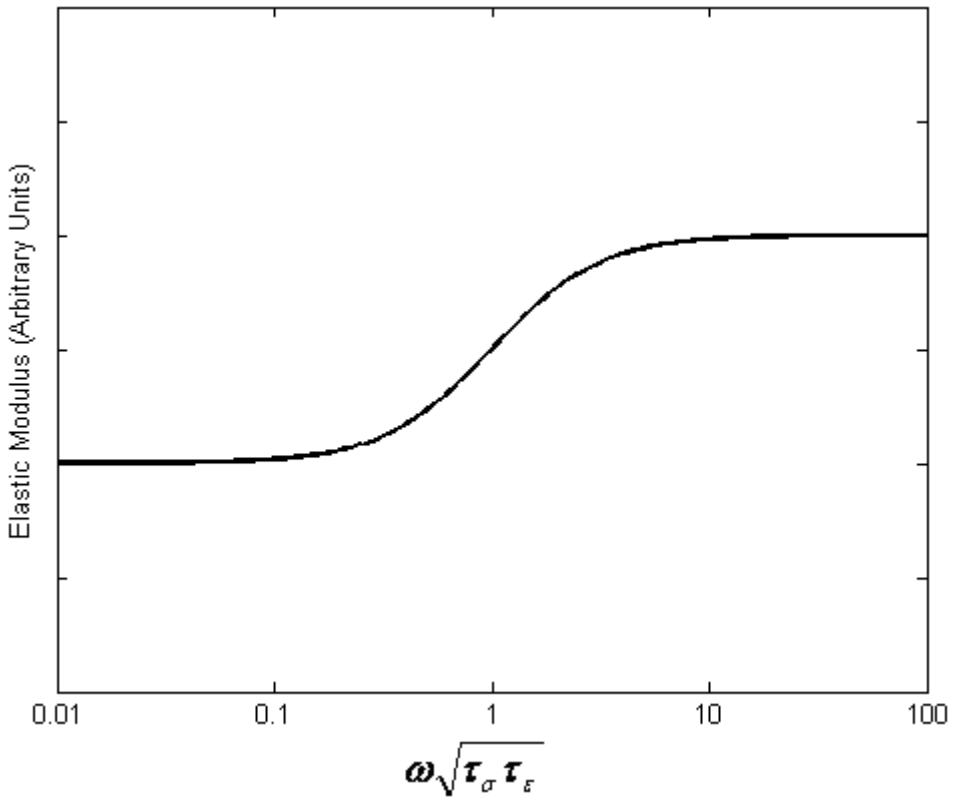

Figure 4.3 The relationship between modulus and frequency for viscoelastic materials. See text for explanation. Modified from Fung (1993)

The creep time is the time constant of the strain response of a tissue after a sudden change in the applied stress. A reasonable estimate of this time can be obtained from the following equation when the strains are assumed to be small (Fung, 1993):

$$\tau_\sigma \approx \frac{\varphi d^2}{\pi^2 Y_M \kappa (1-\varepsilon)} \tag{4.2}$$

where φ is the fluid volume fraction (assumed to be 0.7, see Section 4.5.2.2), d is the thickness of the tissue (ranges from approximately 0.1 mm to 5 mm), Y_M is the elastic modulus (see Section 4.4.2.2), κ is the hydraulic permeability, and ε is the initial strain (assumed to be 0). The only parameter in this equation that has not yet been discussed is the hydraulic permeability; previous studies have shown that typical values of this parameter for soft tissues is on the order of 10^{-15} $m^4/s/N$ (Heneghan *et al*. 2008). Inserting

this value into the above equation results in a creep time on the order of 100 seconds, and consequently a critical frequency on the order of 0.01 Hz. Clearly, even though the simulations in this section of the research assume that the probe tone is of low frequency, it is much higher than 0.01 Hz and it is not justifiable to neglect the effect that a dynamic input will have on the modulus of the tissues.

Looking again at Figure 4.3, it is clear now that these simulations take place at frequencies much higher than the critical frequency and therefore the Young's modulus values must be increased. However, the exact amount of this increase is dependent on the tissue and is not explicitly stated by Fung. Research done by Decraemer on human TMs showed that the modulus is approximately twice as large at higher frequencies (~100 Hz) as at lower frequencies (~0.01 Hz) (Decraemer *et al.* 1980). Therefore, for the remainder of this work, the moduli of the canal walls and TM will be doubled, so the final ranges to be tested are 60 – 180 kPa and 1.2 – 4.8 MPa respectively.

4.4.2.4 OSSICLES AND LIGAMENTS

For the Young's moduli of the ossicles and their ligaments, once again there are no experimental measurements done on newborns in the literature. However, a single modulus will be estimated for each of these structures rather than a range of potential values. This distinction can be made since these parameters are much less important for admittance results in these models than are the moduli of the ear canal and TM (Qi *et al.* 2008). Therefore, as long as the moduli of the ossicles and ligaments are reasonable estimates, the accuracy of the results should be maintained. The Young's modulus of the ossicles will be taken as 3 GPa, as this is slightly below the value used for adult middle-ear models (Koike *et al.* 2002). The Young's modulus of the ligaments will be set to 3 MPa, which assumes that the ligaments have a stiffness similar to that of the TM itself. The logic behind these choices for the modulus values is the same as that of Qi *et al.* (2008).

4.4.2.5 TYMPANIC-MEMBRANE THICKNESS

Unlike the rest of the structures in the models, the TM is built from shell elements rather than solid elements. In other words, it is built as a 3D surface of triangles rather than as a solid volume of tetrahedra. The reason for this distinction is the very small thickness of the TM relative to the remainder of the model. If the TM was in fact meshed as a volume instead of as a sheet, then the aspect ratio of its elements would be extremely skewed and numerical problems would likely occur in the simulations. Shell elements in FEM utilize a different formulation than do the solid elements, allowing the user to specify the desired thickness of the surface as a parameter.

To this date, only a single study has been done on the thickness distribution of the newborn TM. Ruah *et al.* (1991) found that the TM is significantly thicker in the newborn than in the adult, and that the posterior-superior quadrant is significantly thicker than the other three. Therefore, this model attempts to recreate this measured TM morphology by having the thickness of the posterior-superior quadrant set to 0.5 mm and the thickness of the remainder of the TM set to 0.15 mm. (After this thesis had been written, examined and passed, it was discovered that the middle-ear model had the anterior-superior quadrant of the TM as the thickest rather than the posterior-superior quadrant. Some implications of this error are discussed in Section 6.2.2.)

4.4.2.6 MESH RESOLUTION

The mesh resolution of the model is an important parameter that plays a large role in the validity of the results. As mentioned previously, increasing the mesh resolution should result in a monotonic and asymptotic increase in the model displacements and in their accuracy, but also an increase in the computation time. Therefore, it is important to find a resolution that provides a good trade-off between these two factors. In their work, Qi *et al.* used several different resolutions in the ear-canal model in order to determine which one was the most suitable. They found that an increase from 15 to 18 elements per diameter resulted in a 5% increase in displacement magnitudes, whereas an increase from

18 to 22 elements per diameter resulted in less than a 1% increase and a significantly longer computation time. Hence, they decided to use 18 elements per diameter for the remainder of their simulations. In similar fashion, they found that for the middle-ear model, the optimal resolution was 160 elements per diameter for the TM and 40 elements per diameter for the ossicles and ligaments. Since this work utilizes the same models and in this section also involves static simulations, the same resolution is used. Table 4.1 contains a summary of the final material properties to be used for low-frequency simulations.

Simulated Material Properties (Low-Frequency)

	Soft Tissue	**TM (3/4)**	**TM (1/4)**	**Ossicles**	**Ligaments**
Young's Modulus	60-180 kPa	1.2-4.8 MPa	1.2-4.8 MPa	3 GPa	3 MPa
Poisson's Ratio	0.475	0.475	0.475	0.475	0.475
Thickness	—	0.15 mm	0.5 mm	—	—
Resolution (elements/diameter)	18	160	160	40	40

Table 4.1. Summary of material properties for low-frequency simulations.

4.5 DYNAMIC SIMULATIONS

4.5.1 INTRODUCTION

Using static simulations, the behaviour of the newborn ear canal and middle ear can be simulated for low-frequency stimulation. Studying the behaviour at higher frequencies requires a dynamic model that includes inertia and damping. With a dynamic model that is valid at higher frequencies, a much greater understanding of the newborn's ear mechanics can be obtained and the results could potentially suggest a more efficient method of performing tympanometry in newborns. The overall goal of this part of the research is to transform the static model from the previous section into a dynamic model that can describe the system behaviour at higher frequencies.

4.5.2 MATERIAL PROPERTIES

4.5.2.1 OVERVIEW

In addition to the Young's modulus values that are taken from the previous section, density and damping parameters must also be included for all of the materials in the models. For the ear-canal model, the only type of material that is present and free to move is the soft tissue and elastic cartilage that surrounds the canal wall. In the middle ear, there are three different material types: the TM, the ossicles, and the ossicular ligaments.

4.5.2.2 DENSITY

The densities of the model materials can be estimated by analysing the anatomical structures of the various tissues. The overall compositions of the canal soft tissue, the elastic cartilage, the TM and the ossicular ligaments are very similar. Each of these tissues is composed of 60-80% water while the remaining solid structure largely consists of a collagen matrix (Widmaier *et al.* 2006). Since water has a density of 1.0 g/cm^3 and the density of collagen has been measured to be approximately 1.2 g/cm^3 (Harkness *et al.* 1961), then it is logical to assume that the density of all these tissues lies somewhere between these two values (Funnell and Laszlo 1982). Therefore, for these simulations, the density of these materials will be set to 1.1 g/cm^3.

The ossicles are comprised of bone and therefore will have a different density than the rest of the tissues. Skeletal bone can be anatomically broken down into two distinct types: cortical bone and trabecular bone. Cortical bone is the solid white substance on the exterior of a bone; it has a density of approximately 2 g/cm^3 and accounts for approximately 80% of the bone's total weight. Trabecular bone, meanwhile, is a soft and spongy substance located in the interior portion of the bone; it has a density of approximately 1.7 g/cm^3 and accounts for the remaining 20% of the bone's mass (Steele *et al.* 1988). Although these fractions will vary according to the type of bone and

the maturity of the bone, the density of a newborn's ossicles will likely lie in this range between 1.7 and 2.0 g/cm^3. Therefore, the density of the ossicles in these simulations will be set at 1.9 g/cm^3.

4.5.2.3 DAMPING RATIO

The second additional material parameter that needs to be added for dynamic simulations is the damping. As explained previously in Section 3.3, this research will use a Rayleigh damping formulation where the required parameters are a stiffness damping parameter and a mass damping parameter. However, these values cannot be measured directly, but must rather be extrapolated from the damping ratio of the material at different frequencies. Unfortunately, much like for the Young's modulus, there is very little known about the damping ratio of the relevant structures of the newborn ear. Although not specifically performed on newborn tissues, several papers on structures such as soft tissue and temporal bone have suggested that typical human body damping ratios lie in the range from 0.15 to 0.4 (Keefe *et al.* 1993, Dhar *et al.* 2007, McGarry *et al.* 2008). Due to the uncertainty in this parameter and how it depends on the input pressure frequency, two different types of simulations are run with two different damping-ratio distributions, as described in the following section.

4.5.3 TYPES OF INPUT PRESSURE SIGNALS

The first type of simulation uses single-frequency sine-wave input pressures. The frequency of the input given a value in the range from 50 to 2000 Hz, and the admittance of the model is calculated at the end of each simulation. The upper limit of input frequencies is set in order to maintain the validity of the assumption that the ear canal can be modelled as a lumped acoustical element (Shanks and Lilly, 1981). If the input sound frequency is too high, then the wavelength of the pressure will be comparable to the dimensions of the canal itself and the pressure will not be uniform inside the canal. For example, at input frequencies of approximately 5000 Hz, the wavelength of sound in air is approximately 70 mm, which is only 3 times the longest dimension of the canal.

Therefore, our simulations will not use input frequencies in excess of 2000 Hz, to allow for the use of a uniform canal pressure.

Due to the nature of Rayleigh damping, the mass and stiffness damping parameters must be altered when the frequency of the input changes in order to maintain a constant damping ratio. Therefore, using single-frequency inputs, the damping ratio is held constant at 0.25 across all frequencies. This value is chosen because it is near the geometrical mean of 0.15 and 0.4.

The second type of simulation tests all of the frequencies in the appropriate range at once through the use of a step input pressure function. The derivative of the system's step response is its impulse response, and the Fourier transform of the impulse response results in the frequency response. Therefore, the step function allows for the admittance to be calculated at each of the frequencies of interest using the result of a single simulation. This is the major advantage of this technique since it greatly reduces the total number of required simulations. However, this implies that the same mass and stiffness damping parameters will be applied at all frequencies, and therefore the damping ratio will vary with frequency. The mass and stiffness parameters are chosen to be $\alpha = 150$ and $\beta = 4\times10^{-5}$ respectively, resulting in a damping-ratio distribution that has a value of 0.25 at 50 and 2000 Hz. An example of the shape of such a damping ratio distribution can be seen in Figure 3.2 and a summary of these new material properties can be seen in Table 4.2.

Typically, before calculating admittance, the simulations must be run until the transient behaviour becomes negligible. However, for the ear-canal model, likely due to the complex geometry of the structure and the large number of degrees of freedom that are present, the transient behaviour can last for a very long time. For example, as shown in Figure 4.4, if 25 cycles of a 1000 Hz sine wave is used as an input for the ear-canal model, the output has not yet reached a steady state by the end of the stimulation. Many additional cycles would be required to reach the steady-state of the ear-canal model, and this would require much more computation time. Within the last 5 cycles shown in Figure

4.4, the largest difference between any two of the peak amplitudes is 6%. Since the model error due to the uncertainty of the material parameters is much larger than 6%, it is concluded that running the ear-canal model for 25 cycles is enough to provide adequate accuracy despite the fact that the transients have not completely died out.

Additional Material Properties (Dynamic)

	Soft Tissues	Ossicles
Density (g/cm^3)	1.1	1.8
Damping Ratio (Sine)	0.25	0.25
Mass Damping (Step)	150	150
Stiffness Damping (Step)	4e-5	4e-5

Table 4.2. Summary of additional material properties for dynamic simulations. Sine and Step signify the two different types of signal input.

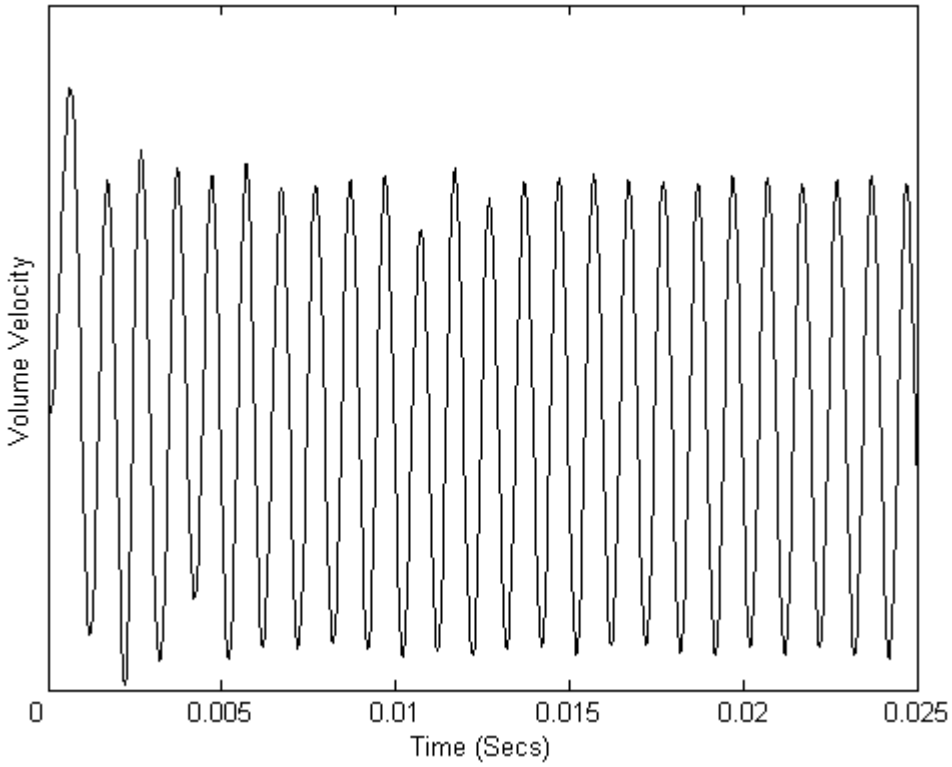

Figure 4.4 Response of the ear canal to 25 cycles of a 1000 Hz sine wave. The response has not reached a steady-state after 25 oscillations.

CHAPTER 5: RESULTS

5.1 INTRODUCTION

In this chapter, the simulation results for both the low-frequency and dynamic simulations of the ear canal and middle ear will be presented. Displacement maps will be shown, the results will be compared to experimental data, and the relative admittances produced by the canal walls and the middle ear will be discussed.

5.2 LOW-FREQUENCY RESULTS

5.2.1 DISPLACEMENT MAPS

Once the proper boundary conditions and material properties have been put in place, *COMSOL* is used to perform the simulations on the ear-canal and middle-ear models. Sample displacement results can be seen in Figures 5.1 − 5.4. For the ear canal, as expected, the majority of the displacement is focused around the boundary of the canal, with the maximum displacement located slightly inferior and lateral to the clamped TM. In the lateral portion of the canal, the displacements seem to be focused on the anterior and posterior walls before shifting more towards the inferior wall in the medial portion. This might be explained by the fact that the ear canal's opening is elongated in the superior-inferior direction in the lateral portion of the canal.

For the middle ear, the displacements are maximal in the inferior-posterior quadrant of the TM, perhaps because of the fact that out of the three thinner quadrants, this region is the largest. Consequently, its centre will be the least affected by the clamped tympanic ring and the mass of the malleus. Displacements are also seen on the manubrium, the head of the malleus, and the long process of the incus.

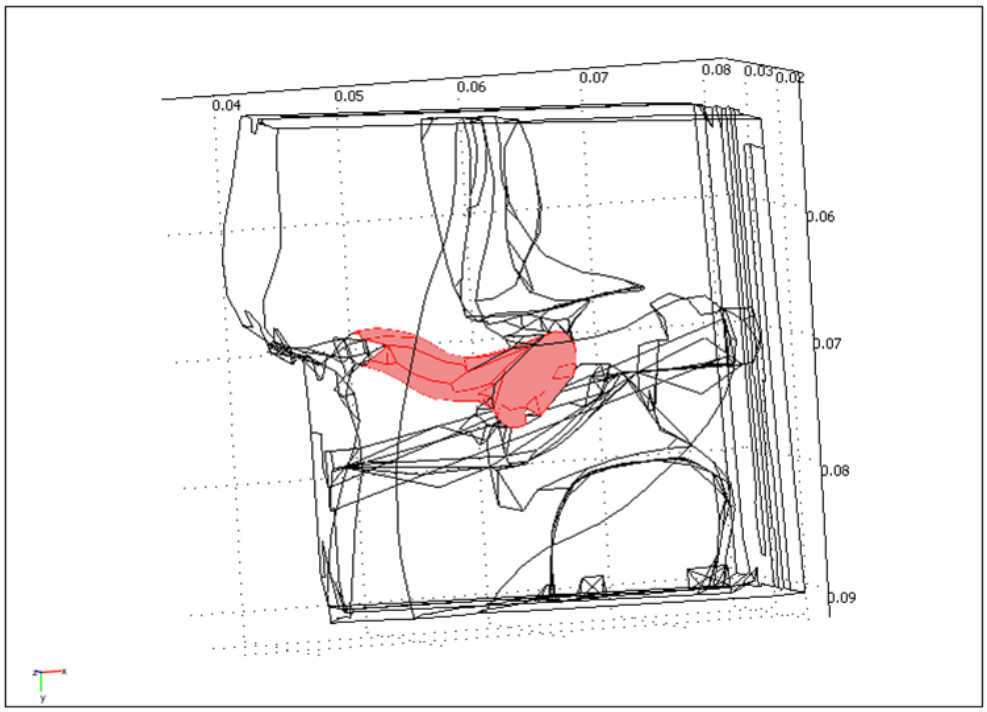

Figure 5.1 View of ear-canal model before simulation. The coloured area represents the walls of the canal where the pressure is applied.

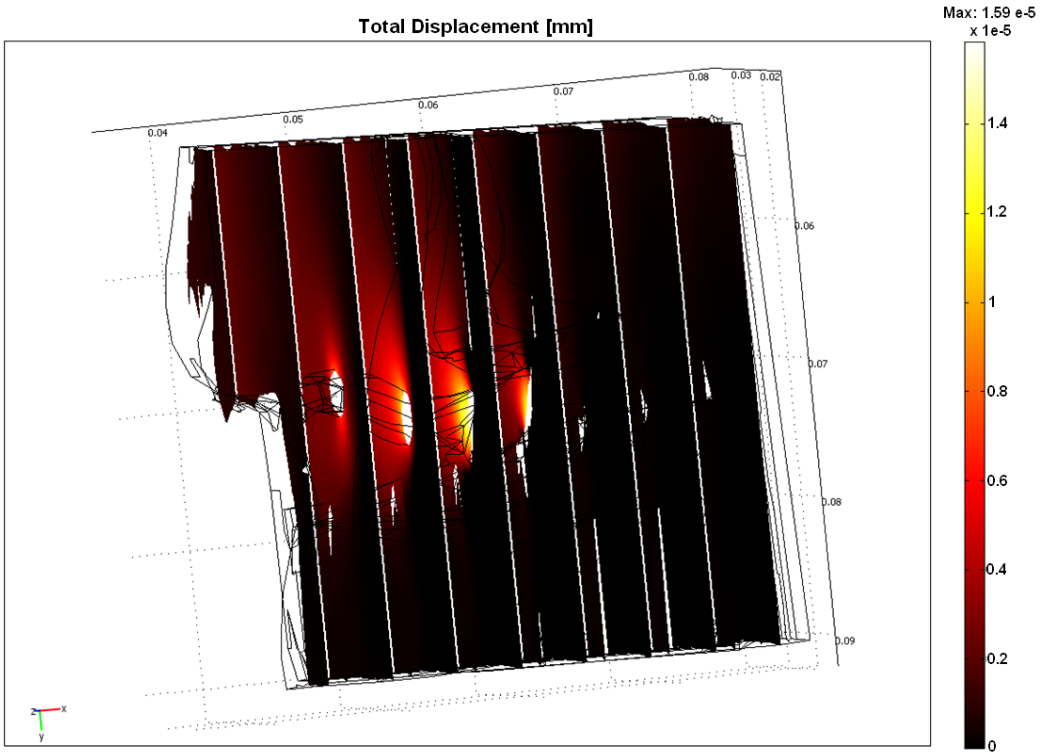

Figure 5.2 Displacement results of ear-canal model. Larger displacements are focused on the canal boundary.

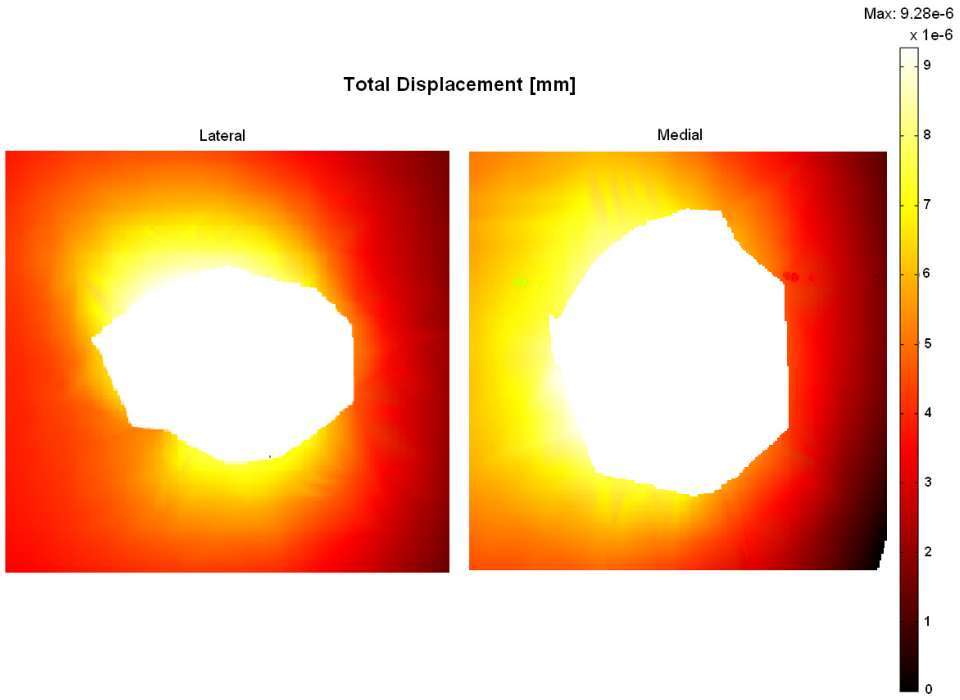

Figure 5.3 Cross-section view of ear-canal model after simulation. Area in white is the canal opening. The displacement pattern of the canal wall changes as the canal is traversed medially towards the TM.

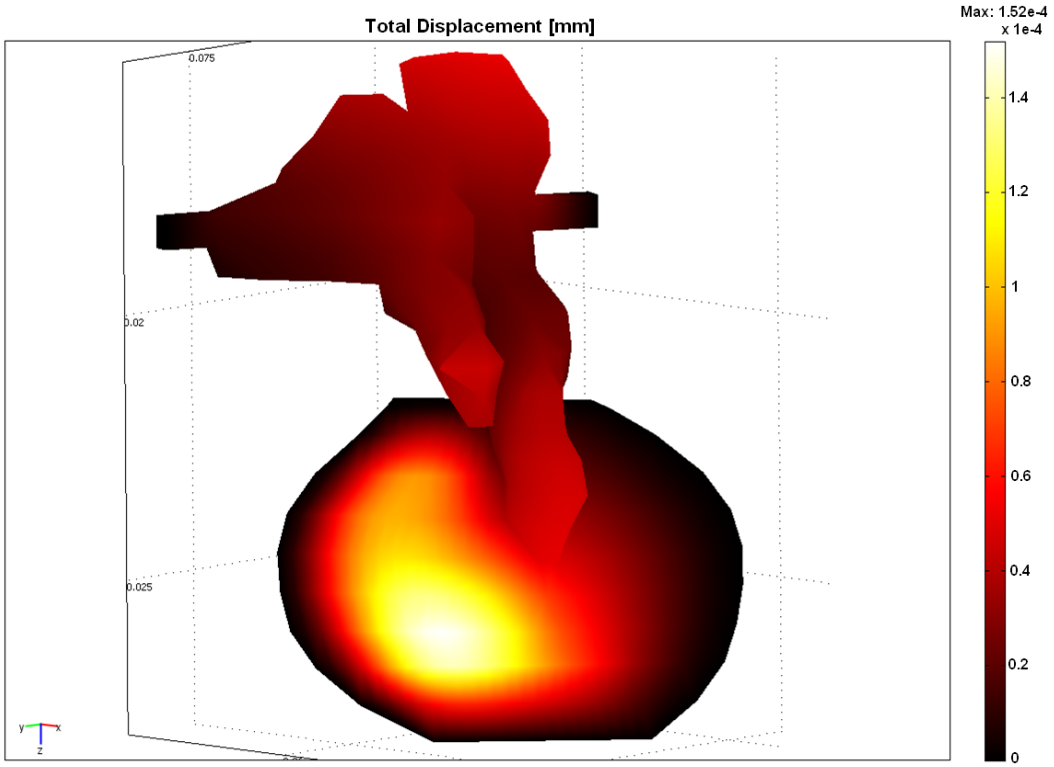

Figure 5.4 Middle-ear simulation results. The displacements are focused primarily in the inferior-posterior quadrant of the TM.

5.2.2 COMPLIANCE CALCULATION

The purpose of these simulations is to study the relative magnitude of the admittances that would be attributed to the ear canal and middle ear in response to a tympanometric probe tone. However, admittance is a dynamic measurement that involves the volume velocity of the structures while these static simulations reveal no dynamic results whatsoever. Therefore, in order to estimate admittance from these results, the following equation will be used to describe admittance at very low frequencies (Keefe *et al.* 1993):

$$Y = j\omega(C_v + C_m + C_w) \tag{5.1}$$

where C_v, C_m, and C_w are the compliances of the ear-canal air volume, the middle ear and the canal walls respectively. In this case, the compliance is defined as the volume change induced by 1 Pa of pressure. This low-frequency admittance is purely imaginary and always positive, implying that the admittance response is at a phase angle of 90 degrees. This coincides with what is expected in a static simulation where the system will be affected only by stiffness. More importantly, the equation also implies that the relative magnitudes of the admittances of the three components are the same as the relative magnitudes of their compliances. Therefore, even when using static simulations, the admittance of the ear in response to a low-frequency probe tone can be determined.

C_v is not a quantity that can be extracted directly from the simulation, but it can be derived explicitly from the following equation (Keefe *et al.* 1993):

$$C_v = \frac{V}{\rho c^2} \tag{5.2}$$

where V is the volume of air in the ear canal, ρ is the density of air (1.2 kg/m^3), and c is the speed of sound in air (343 m/s). Qi *et al.* (2006) calculated the volume of this ear

canal to be 150 mm^3. Using this value, the compliance of the canal air is calculated to be 1.1 mm^3/Pa.

Unlike C_v, both C_m and C_w can be measured directly from the simulation results by calculating the volume displacement corresponding to the displacements generated by the input pressure. The volume displacement (ΔV) of each structure is calculated with the following equation:

$$\Delta V = \sum_{i=1}^{N} d_i \cdot n_i \tag{5.3}$$

where d_i and n_i text are the displacement and normal vectors of the triangular boundary elements i = 1…N that outline the structure of interest, in this case the canal wall and the TM. The dot product must be taken between the displacement and the normal of each boundary element to ensure that shear displacements are not included in the overall integration, since surface displacements that are parallel to the original surface do not produce a volume change.

Using this equation, the total volume displacements of the canal and TM in response to several different input pressures are calculated and plotted in Figure 5.5 and the resulting compliance results are seen in Table 5.1. Clearly, and as expected due to the linear nature of the materials, these curves are all linear and the compliances (slopes of the lines) are inversely proportional to the Young's moduli of the tissues. Although the magnitude of the pressure in calculating stiffness does not matter in a linear system, the input pressure levels are kept around 0.4 Pa (~85 dB) since this is the normal amplitude of the probe tone. The canal-wall and TM compliances seen here are similar to those calculated by Qi et al. (2006, 2008) for the same Young's moduli at the lower limit of their input pressures, where their hyperelastic materials were behaving linearly. The C_w values of 0.0073, 0.0037, and 0.0024 mm^3/Pa are the true canal-wall compliance values that would be used in Equation 5.1. However, this is not the case for the middle-ear model. The FEM simulations of the middle ear do not take the effect of the middle-ear

cavity into account, and many studies have shown the large impact that this cavity can have on the admittance of the middle ear (e.g., Zwislocki *et al.* 1962, Funnell and Laszlo 1982, Stepp and Voss 2005). Therefore, the calculated middle-ear compliance values must be adjusted in order to compensate for this effect.

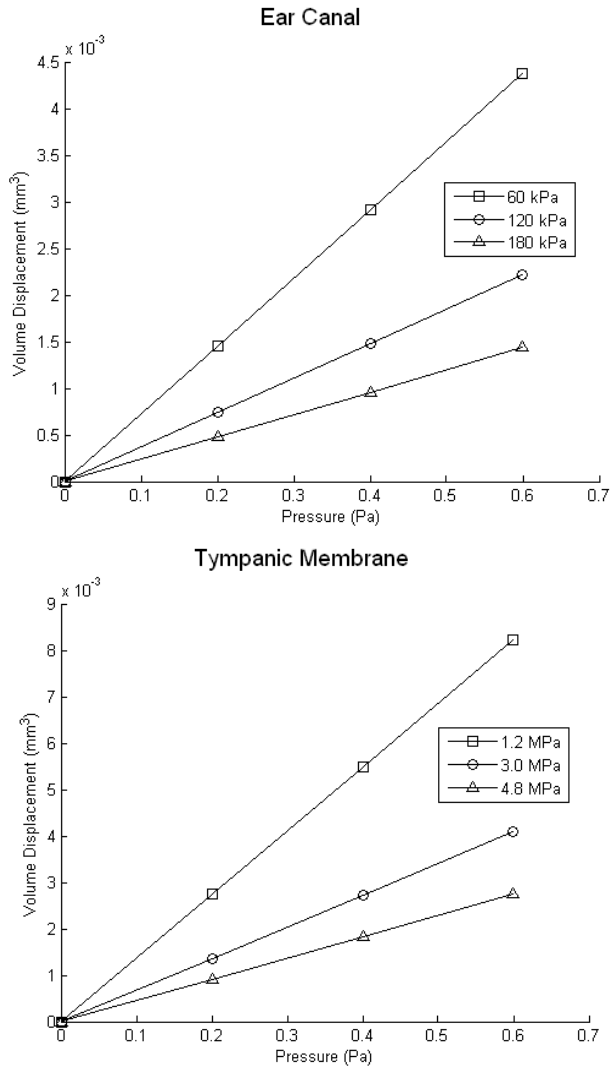

Figure 5.5 Volume displacement versus pressure curves for ear canal and TM for different Young's moduli

Ear-Canal Compliance (mm^3/Pa)

60 kPa	120 kPa	180 kPa
0.0073	0.0037	0.0024

TM Compliance (mm^3/Pa)

1.2 MPa	3.0 MPa	4.8 MPa
0.014	0.0068	0.0046

Table 5.1 Compliance results for ear canal and TM for different Young's moduli

5.2.3 ACCOUNTING FOR MIDDLE-EAR CAVITY

The alteration in the compliance of the middle ear due to the cavity is caused by the air that is trapped in this space. As the TM gets displaced inward, for example, the air on the medial side of the TM is compressed and exerts a force back on the TM. This effect can be modelled as an impedance element (Z_{CAV}) in series with the impedance of the TM itself (Z_{TM}) (Stepp and Voss, 2005):

$$Z_{ME} = Z_{TM} + Z_{CAV} \tag{5.4}$$

where Z_{ME} is the total impedance of the middle ear that would be detected in tympanometry. Conversion of the above equation from impedance to compliance results in

$$\frac{1}{C_{ME}} = \frac{1}{C_{TM}} + \frac{1}{C_{CAV}} \tag{5.5}$$

The equation for the compliance of the air in the middle-ear cavity (C_{CAV}) takes the same form as Equation 5.2 for the ear-canal volume. Consequently, an estimate is needed for the volume of the cavity itself. However, before this estimation is performed, it is important to realize that the middle-ear cavity can be in one of two different states.

As described in Section 2.7, the Eustachian tube connects the middle-ear cavity to the nasal cavity and can be in either an open or a closed state. When it is open, the middle-ear cavity, for the purpose of calculating compliance, would essentially extend into the nasal cavity and out into the air surrounding the body. In this case, it is very reasonable to assume that the cavity is infinite in volume. This leads to the air compliance being infinite as well, resulting in the cavity having a negligible effect on the admittance. Simply put, if the Eustachian tube is open, then the air is free to move in and out of the middle-ear space. Therefore, the air exerts no force since it does not get compressed or decompressed when the TM displaces. This situation, however, when the Eustachian tube is open and the middle-ear cavity is directly connected to the external air, is rare. The tube generally only opens for brief intervals during yawning, swallowing, etc., and so it is much more likely that the tube will be closed when tympanometric data are being recorded. The open-cavity situation tends to arise more often during *post mortem* experiments when a hole has been drilled in the temporal bone.

For the purpose of this model, it is assumed that the simulations are run when the Eustachian tube is closed. Therefore, an accurate estimate of the newborn's middle ear cavity volume is needed to determine its effect on the middle-ear admittance. Qi *et al.* (2008) estimated this volume as being between 700 and 1000 mm^3 using the CT segmentation data. Subsequently, in this research, it will be assumed that the cavity has a volume of either 700 or 1000 mm^3 in order to provide limits on this cavity's effect. These cavity volumes result in an air compliance of 0.0050 and 0.0071 mm^3/Pa respectively. Using these compliance values in Equation 5.5 leads to a drastic change in the total middle-ear compliance values as seen in Table 5.2. Not only does the closed cavity decrease the compliance of the middle ear by almost 75% in some cases, but it also eliminates the inversely proportional relationship between the middle-ear compliance and the Young's modulus of the TM. In fact, the addition of the middle-ear cavity reduces the ratio between the middle-ear compliance at the minimum and maximum modulus from 3 to 1.6. Therefore, the cavity causes the results of the simulation to be much less sensitive to the Young's modulus of the TM, a convenient outcome due to the uncertainty in this parameter's value.

Middle-Ear Compliance (mm^3/Pa)

	1.2 MPa	3.0 MPa	4.8 MPa
Open Cavity	0.014	0.0068	0.0046
Closed Cavity (700 mm^3)	0.0037	0.0029	0.0024
Closed Cavity (1000 mm^3)	0.0047	0.0035	0.0028

Table 5.2. Middle-ear compliance results for different Young's moduli including the effects of the middle-ear cavity

5.2.4 COMPARISON WITH EXPERIMENTAL DATA

With the compliance values calculated and external effects accounted for, the simulation results are validated via comparison to experimental results. Due to the uncertainty of the Young's moduli of the system, the total simulated compliance of the ear is expressed as a range. The upper boundary of the range corresponds to moduli of the canal wall and TM of 60 kPa and 1.2 MPa respectively at a middle-ear cavity volume of 1000 mm^3, while the lower boundary of the range corresponds to moduli of 180 kPa and 4.8 MPa respectively at a middle-ear cavity volume of 700 mm^3. The compliance of the canal air is independent of these parameters and is therefore held constant at a value of 0.0011 mm^3/Pa. Using these criteria, it is concluded that the simulated total ear compliance is 0.0059-0.0131 mm^3/Pa. The data that will be used for comparison will be from Keefe *et al.* (1993) where they measured the impedance of the ear for normal subjects in a variety of different age groups. They used phase information to separate the impedance into resistance and reactance and then used the following formula to convert input reactance (X_{in}) to input compliance (C_{in}):

$$C_{in} = \frac{-1}{\omega X_{in}} \tag{5.6}$$

Their averaged reactance measurements and the derived compliances for the group of fifteen 1-month-old newborns can be seen in Figure 5.6. For this subject group, the compliance plot suggests that the average total low-frequency ear compliance is

approximately 0.007 mm^3/Pa. However, the lowest frequency represented on this plot is 250 Hz, and it is possible that this is not an accurate representation of the true low-frequency behaviour. Looking at the reactance plot instead, the minimum frequency in this data set is 125 Hz. Reading the data off the graph, the average reactance of the newborn ear at 250 Hz is approximately -900 CGS ohms while the average reactance at 125 Hz is approximately -1900 CGS ohms. Using these two values in Equation 5.6 gives compliance values that differ by only 5%. Therefore, due to the nearly identical compliances seen at 125 and 250 Hz, it is assumed that 0.007 mm^3/Pa is indeed the experimental low-frequency ear compliance. This value lies within the simulated range and thus indicates that the model is consistent with the measured data

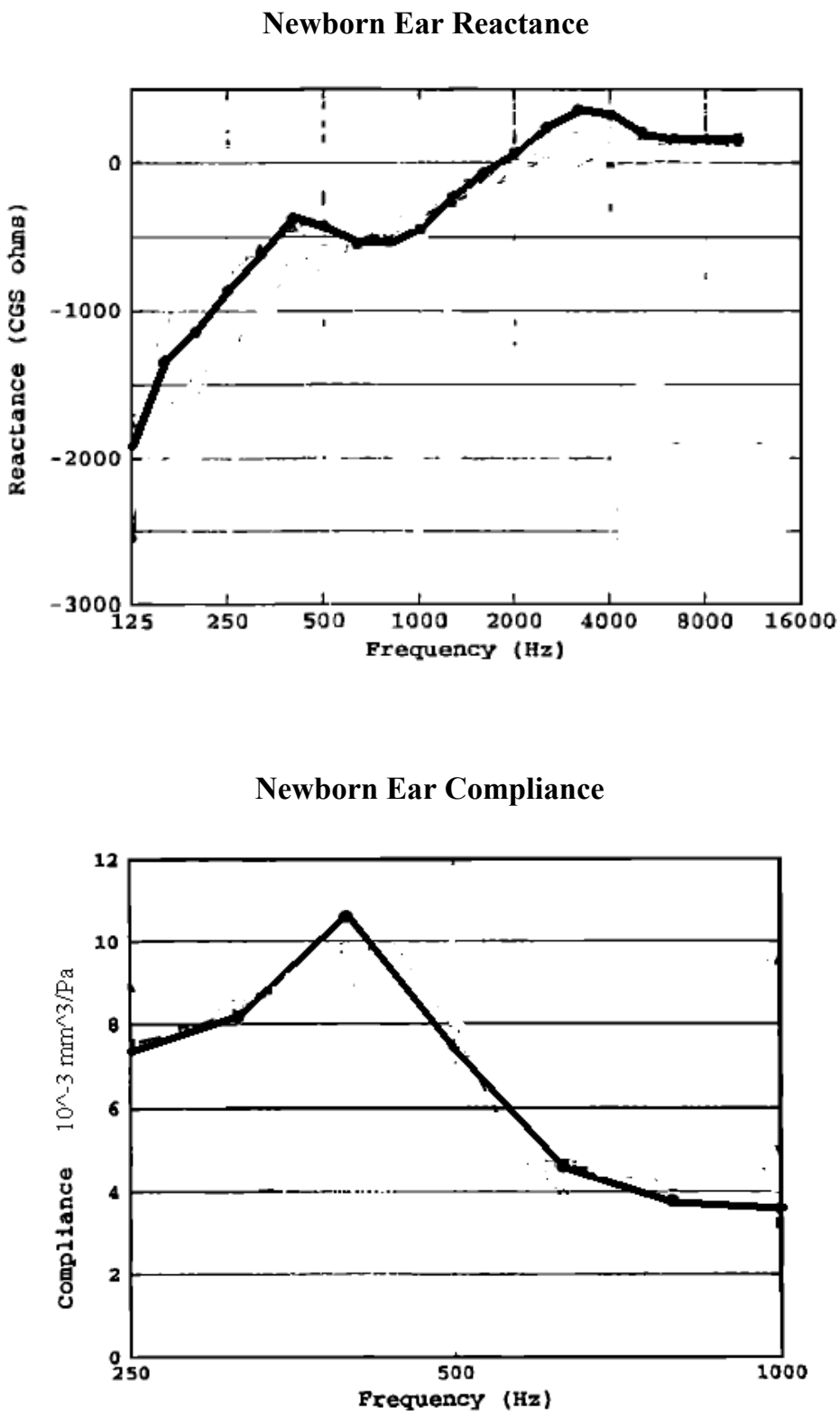

Figure 5.6 Experimental newborn ear measurements used for model validation. Modified from Keefe (1993)

5.2.5 RELATIVE COMPLIANCE

With the model producing overall compliance results similar to those seen in the measurements of Keefe *et al.*, the individual compliance values that comprise the total value are now analyzed separately. This is an analysis that cannot be done experimentally; the tympanometer cannot distinguish between the admittance of the canal and that of the middle ear. The simulated compliance of the newborn ear-canal air volume, ear-canal wall, and middle ear for the open middle-ear cavity state as well as both closed-cavity volumes are seen in Figure 5.7. The two different graphs use the lower and upper limit of the Young's moduli respectively. As can be clearly seen, in the closed-cavity state the compliance of the newborn's canal wall is very similar to the compliance of the middle ear. Even for the open-cavity state of the middle ear, even though the middle-ear compliance value has been increased significantly, it is still unreasonable to deem the canal-wall displacements negligible in this situation.

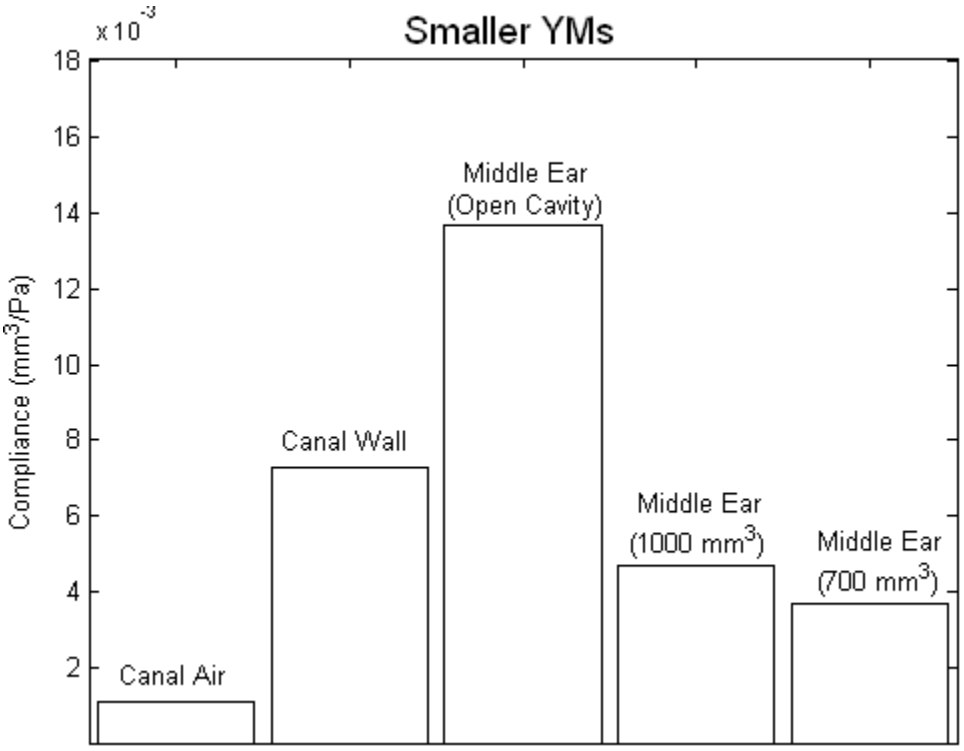

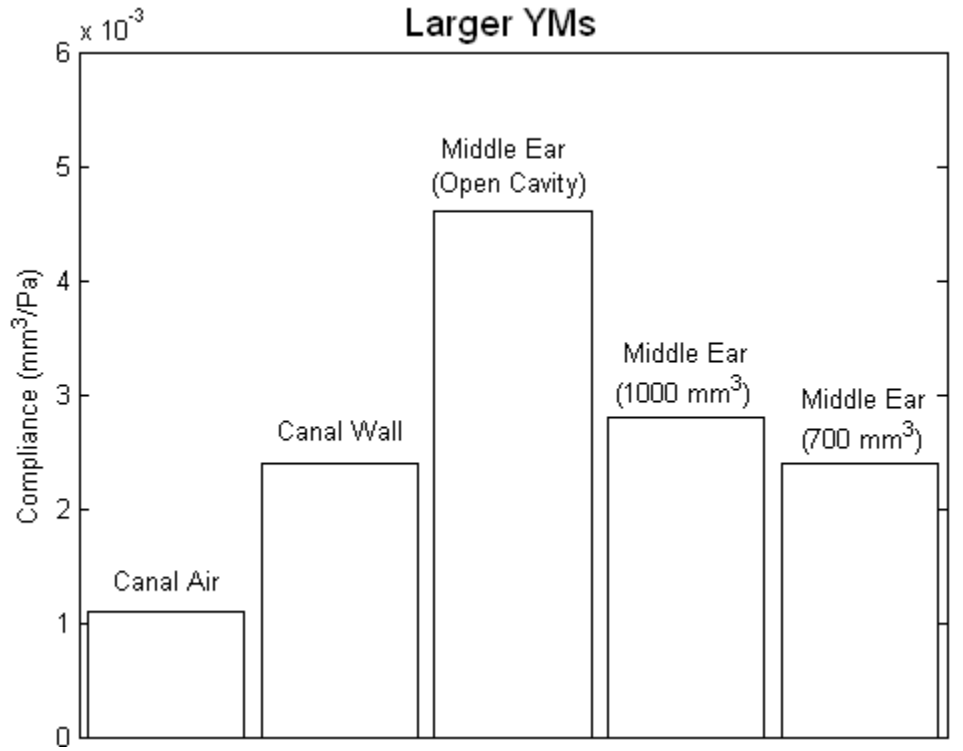

Figure 5.7 Comparison of simulated compliances for different Young's moduli.

This observation is drastically different from what is seen in the adult where the compliance of the bony canal wall is typically considered unimportant when compared with that of the middle ear. In the adult, the normal tympanometric procedure is to first isolate the compliance of the air volume by introducing a large static pressure into the ear. After this is done, the second step is to subtract this extrapolated air compliance from the normal results to isolate the response of the middle ear. Both of these steps, however, require the assumption that the canal-wall compliance and admittance are negligible, which is obviously not the case in these simulations for the newborn. If the canal wall is compliant, then the ear-canal volume will change under a large static pressure, skewing the compliance value of the canal air. Also, subtracting this air compliance from the total would result in the combination of the canal-wall and middle-ear signals and not simply the isolated middle-ear value. Apparently, the fact that the newborn's canal wall is not yet fully ossified and has a much lower stiffness than that of the adult plays a large role in the admittance measurement.

5.3 DYNAMIC RESULTS

5.3.1 OVERVIEW

Unlike the static simulations where the velocity-based admittance is estimated from the displacement-based compliance, dynamic simulations allow for the direct calculation of the admittance from the simulation due to the inclusion of the time parameter in the results. The output of interest is the overall volume velocity of the ear canal or TM. During the single-frequency simulations, the resulting volume velocity after transients will be a scaled and shifted version of the input sine wave. The magnitude of the admittance is simply the amplitude of the output wave, while the phase of the admittance can be deduced from the time lag separating the peak of the output and the peak of the input. Conductance and susceptance can then be easily calculated from these measures. The calculation of admittance for the step-input simulations is performed using the Fourier transform of the volume velocity as explained in Section 4.5.3.

5.3.2 CONVERGENCE TESTS

For the static simulations, convergence tests were not performed since Qi *et al.* (2006, 2008) confirmed that the resolution and number of slices in the model were both satisfactory for static tests. However, this may no longer be the case when the model is dynamic, and therefore the effect of resolution needs to be tested. In the middle ear, the number of elements per diameter for the TM is increased from 160 to 200, and the number of elements per diameter for the ossicles and ligaments are increased from 40 to 60. The increase in the resulting displacements varies across the range of input frequencies, but the average increase in amplitude is approximately 4.5%, the maximum increase is less than 7%, and there is no discernible effect on phase at any frequency. Due to the fact there is a large amount of uncertainty in the Young's moduli and damping ratios in this model, it is deemed that the level of accuracy provided by the lower-resolution model is satisfactory. Likewise, the same conclusion is made for the ear-canal model, since when the number of elements per diameter is raised from 18 to 22, the average increase in the displacements is approximately 3%, the maximum increase is less than 6%, and there are no detectable phase differences.

The next convergence test involves the number of slices that need to be included on the inferior side of the ear canal. The model used by Qi included only approximately 3 mm of tissue on the inferior side of the canal since this is the extent of the slices that are included in the CT scan. Through his own convergence testing, he concluded that this is an appropriate number of slices for a static simulation. In order to test this conclusion for dynamic simulations, an additional 6 mm of tissue was added artificially by extrapolating the geometry of the structures on the last slice of the CT scan. The differences between the admittances and phases of the two models, with parameter values at the centres of their ranges, can be seen in Figure 5.8 When comparing the results of the original model to the one with the additional slices, although there are differences of up to 35% between the admittance magnitudes of the two models at some frequencies, the two curves are qualitatively similar. However, there are definite qualitative differences between the phase responses of the two systems. The phase of the model without the additional slices

is negative between the frequencies of 600 and 1000 Hz while the model with additional slices has a positive phase throughout. Hence, the model does not behave appropriately without the added tissue on the inferior side of the canal for dynamic simulations. This may be because a dynamic pressure on the ear-canal walls produces strains that extend deeper into the surrounding tissues than the strains produced by a static pressure. The geometry with the additional slices will be used for the remainder of this study. To ensure that even more slices are not required, a simulation was run with the inferior face of the model clamped in place and there are only very small differences in the results obtained. This demonstrates that any further additions to the inferior side of the structure will have very little effect on the results.

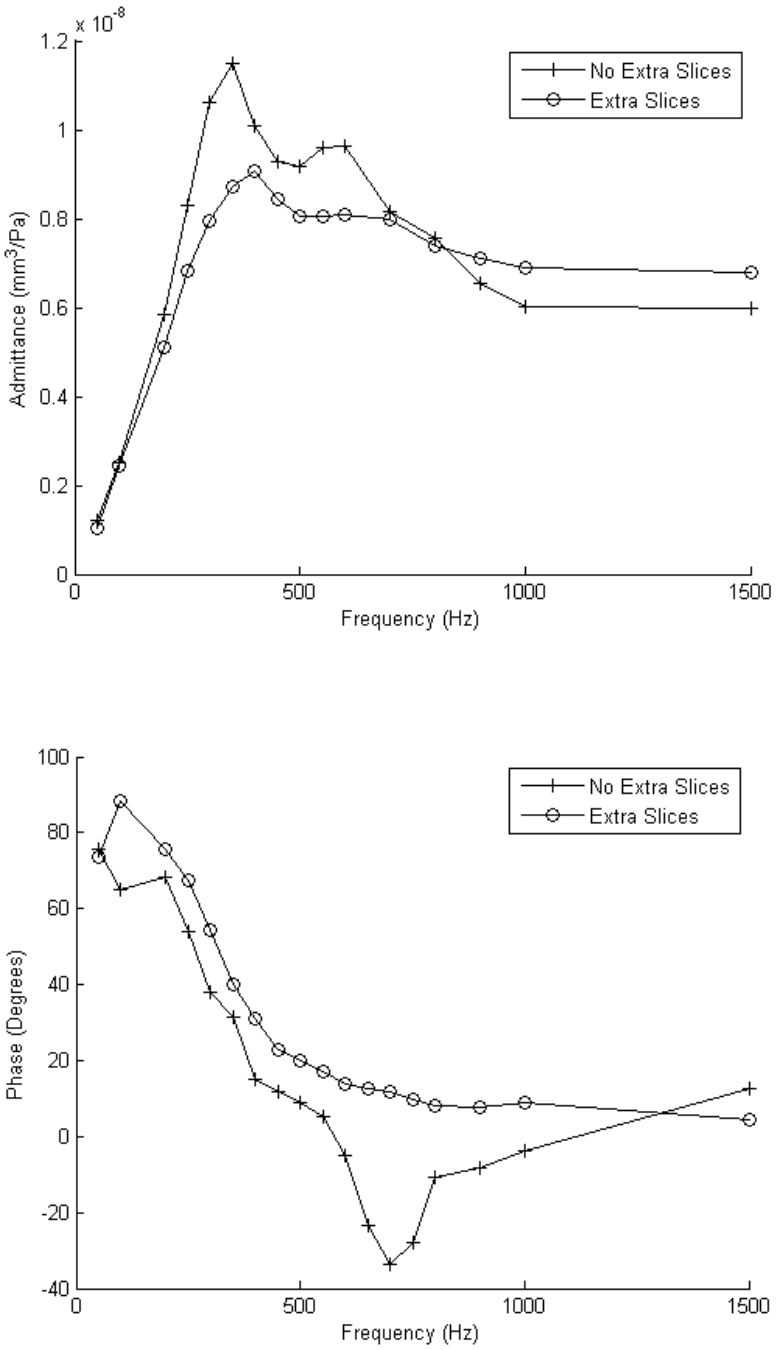

Figure 5.8 The effect of additional inferior slices on the response of the ear canal.

5.3.3 SENSITIVITY ANALYSIS

Due to the large number of parameters present in the dynamic system, a sensitivity analysis is performed to analyze the relative importance of the various parameters. The Elementary Effects Method (EEM), described in Section 3.4, will be used for this analysis since a full global and quantitative analysis is not needed in this case. This is because the results of this sensitivity test will not be used for model updating, but rather for supplying a qualitative description of the importance of the parameters.

Two different outputs will be used to describe the effects of each parameter: the maximum admittance, and the frequency at which this maximum occurs. These two outputs are used because it is very common that a certain parameter change can have a large effect on one and a minimal effect on the other. Single-frequency simulations are used to obtain the values of μ and σ since they allow for the same damping ratio to be simulated at all frequencies. However, the example frequency-response curves are generated with a step-function input since it is more practical to use this method for generating smooth curves.

The primary decision that needs to be made before performing EEM is the range of each of the parameter values. These ranges must be chosen carefully since the sensitivity results are normalized by these range values. For this work, the ranges are based on the uncertainty that may be present in their values due to lack of experimental data or inter-subject variability. For the ear-canal simulations, the three examined parameters are the Young's modulus, density, and damping ratio of the soft tissue. The range of moduli used is the same as in the static simulations ($60 - 180$ kPa), the range of densities used is $900 - 1300$ kg/m^3, and the range of damping ratios used is $0 - 0.5$. This range of damping ratios is larger than the one given in Section 4.5.2.3 since those experimental measurements were not specific to the newborn ear canal.

	Middle Ear				Ear Canal			
	Maximum Admittance ($mm^3/s/Pa$)		Resonance Frequency (Hz)		Maximum Admittance ($mm^3/s/Pa$)		Resonance Frequency (Hz)	
	μ	**σ**	**μ**	**σ**	**μ**	**σ**	**μ**	**σ**
Young's Modulus	−16	6.4 (40%)	290	30 (10%)	0.40	0.13 (33%)	380	185 (49%)
Density	-2	0.2 (10%)	−165	5 (3%)	-0.66	0.13 (20%)	-80	10 (13%)
Damping Ratio	−50	14.2 (28%)	15	15 (100 %)	−0.80	0.09 (7%)	−10	10 (100%)
TM Thickness (3/4)	−32	14.8 (46%)	−50	40 (80%)				
TM Thickness (1/4)	−4	0.8 (20%)	−70	50 (71%)				
ME Cavity Size	4	5.0 (125%)	−110	130 (118%)				

Table 5.3 EEM results for ear-canal and middle-ear models. The percentage in brackets indicates the relative size of σ_i compared to μ_i (σ/μ).

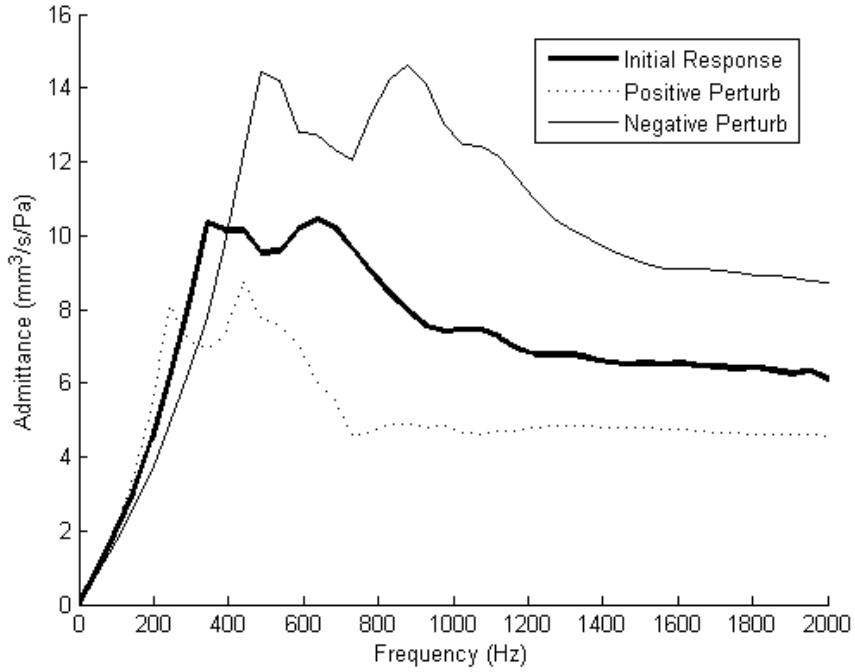

Figure 5.9 Effect of positive and negative density perturbations on the admittance of the ear canal

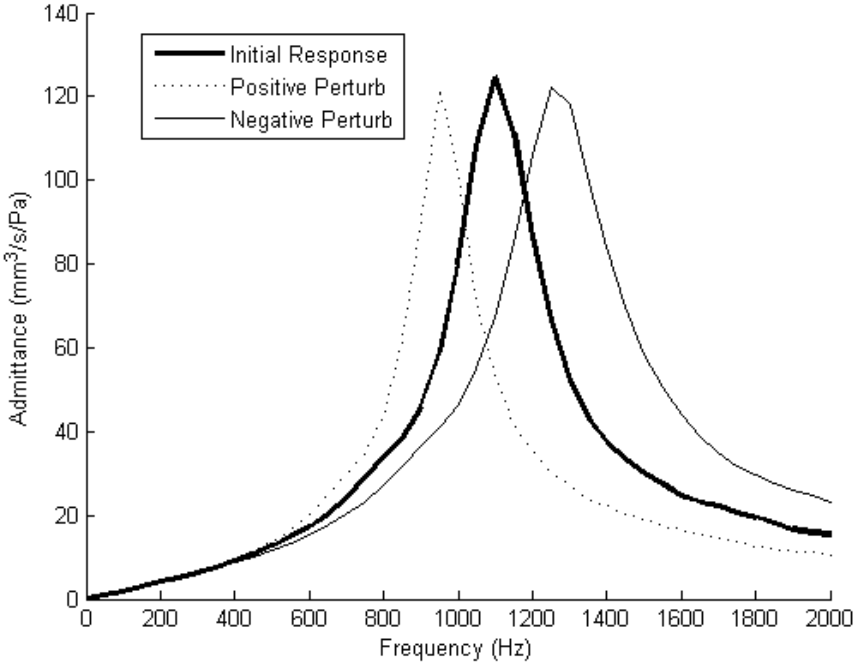

Figure 5.10 Effect of positive and negative density perturbations on the admittance of the middle ear

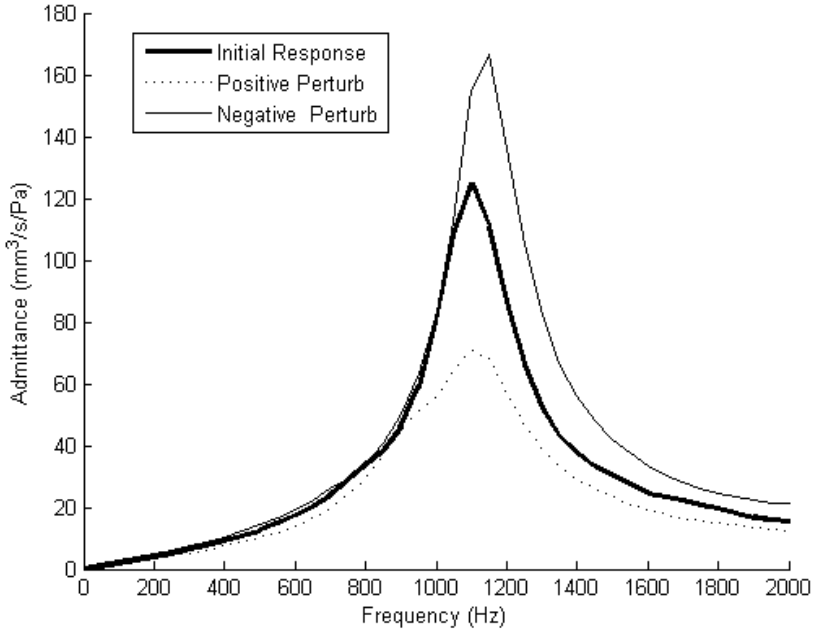

Figure 5.11 Effect of positive and negative thickness perturbations (just the 3 thinner quadrants) on the admittance of the middle ear

With these specifications in place, the EEM procedure from Section 3.4 is carried out on the canal model and the values of μ and σ are presented in Table 5.3. For a simple mechanical problem with one degree of freedom, the damping ratio affects the size of the resonance peak while the stiffness and density affect the location of this peak. However, for this complicated model of the newborn ear with many degrees of freedom, these relationships are not as cut and dried. The exact effect of a density perturbation on the ear-canal frequency response can be seen in Figure 5.9 For example, the density and the Young's modulus have a significant effect on the maximum admittance of the ear canal ($\mu = -0.66$ and 0.40 $mm^3/s/Pa$ respectively). In fact, the density has almost as large an effect as the damping ratio ($\mu = -0.8$ $mm^3/s/Pa$). Looking instead at the resonance frequency of the ear canal, its value is most sensitive to the value of the Young's modulus ($\mu = 380$ Hz), it is moderately sensitive to the value of the density ($\mu = -80$ Hz), and it is almost completely insensitive to the value of the damping ratio ($\mu = -10$ Hz). These effects are similar to what one sees with a simple system. The effect of the Young's modulus acts in a direction opposite to that of the density and the damping ratio for both the maximum admittance and the resonance frequency of the canal. However, it

consistently has a fairly large σ/μ value (33% and 49%), implying that its effect will vary considerably depending on where the model sits in parameter space.

The middle-ear model has several additional parameters that are not present in the ear-canal model, due mainly to the presence of several different types of materials. These new parameters include the Young's moduli, densities and damping ratios of the TM, ossicles and ligaments; the thickness distribution of the TM; and the size of the middle-ear cavity. Preliminary tests showed that reasonably sized changes of the ossicle and ligament material properties had very little effect on the system output and they will therefore be left out of the sensitivity analysis. This finding is consistent with previous findings (e.g. Lilly *et al.* 1984) that tympanometry is relatively insensitive in detecting abnormalities of the ossicles or ligaments. For the middle ear, the ranges of densities and damping ratios are the same as those used in the ear canal; the range of Young's moduli is 1.2 − 4.8 MPa the range of thicknesses in the three thinner quadrants is 0.075 − 0.225 mm; the range of thicknesses in the thicker quadrant is 0.35 − 0.65 mm; and the range of middle-ear cavity volumes is 700 − 1000 mm^3.

The results of the EEM analysis for the middle ear are in Table 5.3. Overall, the maximum admittance of the middle ear is sensitive mainly to changes in the damping ratio (μ = −50 mm^3/s/Pa), the thickness of the 3 thinner TM quadrants (−32 mm^3/s/Pa) and the Young's modulus (−16 mm^3/s/Pa), while it is insensitive to changes in the density (−1.6 mm^3/s/Pa), the thickness of the thicker TM quadrant (−3.6 mm^3/s/Pa) and the middle-ear cavity size (3.8 mm^3/s/Pa). The middle-ear resonance frequency is most sensitive to changes in the Young's modulus (μ = 290 Hz) and the density (−165 Hz), while it is quite insensitive to changes in the damping ratio (15 Hz) and thicknesses of the TM (−50 and −70 Hz).

There are a few observations that stand out from these results. The first is that the distinction between the damping ratio's effect and that of the density and Young's modulus is much more pronounced in the middle-ear model than in the ear-canal model. This may be due to the smaller number of nodes (and therefore degrees of freedom) in the

middle ear. The full effect of a density perturbation on the middle-ear model can be seen in Figure 5.10. Also, most of the μ values for the resonance frequency of the middle ear are quite small, implying that this resonance frequency is likely quite consistent and relatively insusceptible to changes in these parameters. In fact, the only parameters that have a significant effect on the middle-ear resonance frequency are the Young's modulus and density of the TM and the size of the middle-ear cavity. Increasing the thickness of the TM will increase both the stiffness and the mass; since stiffness and mass have opposite effects on a resonance frequency, their effects will tend to cancel and the effects of thickness variations will therefore tend to be small. The thickness of the TM, especially of the three thinner quadrants, plays a significant role in the maximum admittance of the middle ear, as can be seen in Figure 5.11, and also partakes in large non-linear interactions with the other parameters. Finally, the effect of the middle-ear-cavity size is extremely unpredictable as evidenced by the fact that its standard deviation is larger than its mean for both outputs. For example, for one point in parameter space, decreasing the volume of the middle-ear cavity from 950 mm^3 to 800 mm^3 caused the resonance frequency to rise by 60 Hz, whereas at a different point in parameter space, this volume decrease caused the resonance frequency to drop by 10 Hz.

5.3.4 MODEL VALIDATION

In order to validate the results of these models, they are compared with the experimental data measured by Keefe *et al.* (1993). Their data were plotted as average total ear impedance magnitude (in dB) and phase for several different age groups including a group of 1-month old newborns. Although their data were recorded at input frequencies as large as 10 kHz, only the measurements below 2 kHz will be used for validation because our simulations are limited to this frequency (see Section 4.5.3). In order for the model results to be appropriately compared with Keefe's experiment, Keefe's data must first be converted from impedance to admittance. Once this is done, the admittance of the ear-canal walls, the middle ear, and the canal air volume must be combined to form the simulated total ear admittance.

For this comparison, all of the parameter values were at the centres of their ranges except for the Young's modulus and the damping ratio of the TM. These two values were set at 4.8 MPa and 0.4 respectively; these values are at or near the upper limits of their respective ranges, and were chosen to give a better match between the simulated and experimental admittances. The results can be seen in Figures 5.12 and 5.13.

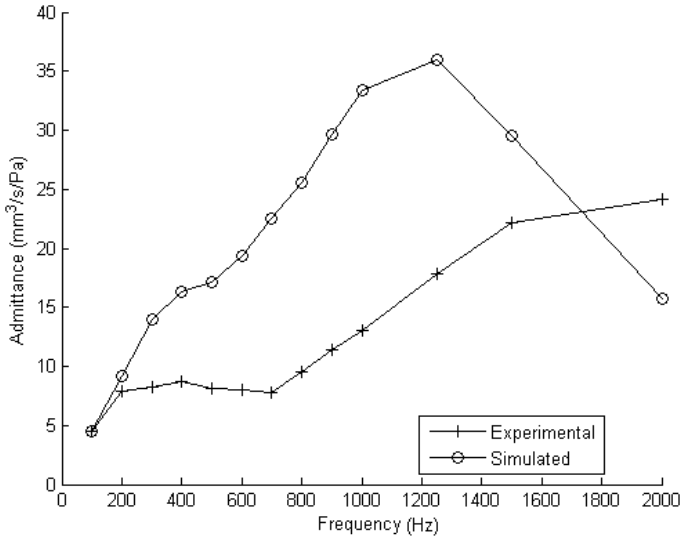

Figure 5.12 Admittance magnitude comparison.

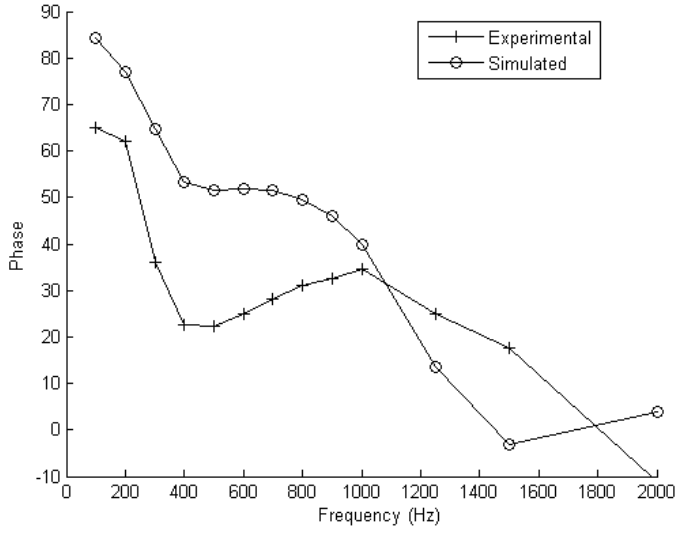

Figure 5.13 Admittance phase comparison.

When comparing the simulated and experimental admittance magnitudes, qualitatively similar features are seen in both curves. The simulated admittance magnitude has an inflection at ~500 Hz and a resonance peak at approximately 1200 Hz. On the other hand, the experimental admittance magnitude of Keefe *et al.* has a broader and more exaggerated version of an inflection in the 200–800 -Hz range, and is consistent with a resonance peak somewhere above 1500 Hz. The experimental and simulated magnitudes match closely at the lowest frequency but at higher frequencies (except the highest) the simulated admittance is higher by a factor of up to ~2.5. A similar degree of qualitative similarity is seen for the admittance phase curves of Figure 5.13. With the large amount of inter-subject variability present in the admittance data of newborns, the simulated results here may not be entirely unrealistic. Moreover, given the large amount of uncertainty in the model parameter values, it may be possible with further adjustments to obtain a much better match with the experimental data with a reasonable set of parameter values.

5.3.5 RELATIVE ADMITTANCE

The primary purpose for performing these simulations is to compare the admittance of the newborn ear-canal wall with that of the middle ear. The comparison of these two values for all frequencies for both the single-frequency and step-function inputs can be seen in Figure 5.14. It is clear that the two different types of input do not produce identical results. The ear-canal curves are very similar for both input types. For the middle ear, the peak is at the same frequency for both input types but the amplitude is much higher for the step-function input. This is presumably because the step-function simulation provides much less damping in the mid-frequencies. However, as mentioned in Section 4.5.3, the damping ratios of these two simulation types are equal when the frequency is either 50 Hz or 2000 Hz; as can be seen in Figure 5.14, the corresponding admittance magnitudes match very well at those frequencies.

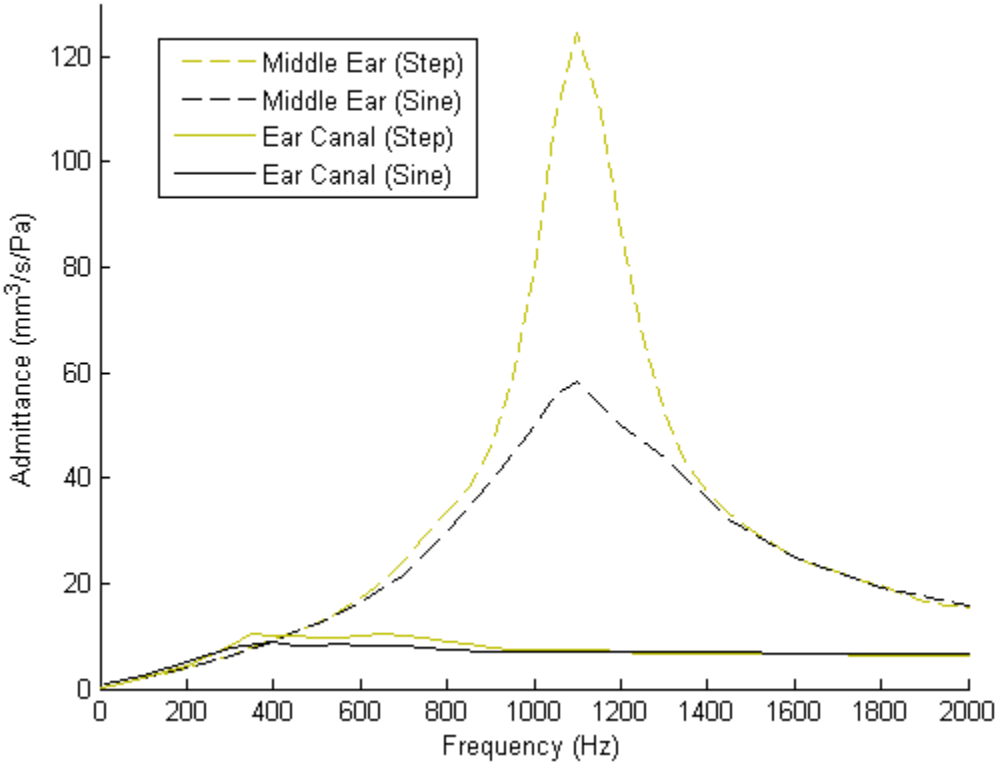

Figure 5.14 Comparison of ear-canal and middle-ear admittances for both sine-wave and step inputs

Despite the differences that are present, these two pairs of curves share some important similarities. At frequencies up to approximately 250 Hz, the admittances of both the middle ear and the canal wall increase linearly with input frequency. This behaviour suggests that for these frequencies the mass and damping of the systems are negligible, and the only parameter of importance is the stiffness of the tissues (see Equation 5.1), which is consistent with the experimental data presented in Section 5.2.4.

The results in this region should match the results seen in the static simulations. In Section 5.2.5, the primary conclusion was that at low frequencies, the admittance of the canal walls and middle ear are comparable in the newborn. Both pairs of curves here are in accordance with this observation. Also, these pairs of curves each give a canal-wall admittance of approximately 5 $mm^3/s/Pa$ at 200 Hz, and if the canal-wall compliance with a Young's modulus of 120 kPa from Table 5.1 is converted to admittance through Equation 5.1, the result is a canal-wall admittance of 4.65 $mm^3/s/Pa$ at 200 Hz. These

results confirm that the dynamic simulations at low frequencies are able to reproduce the behaviour of the static simulations.

Once the input frequency surpasses 250 Hz, the behaviours of both the canal walls and the middle ear begin to incorporate the effects of damping and inertia and the admittance no longer increases linearly with frequency. The admittance of the canal wall plateaus rather quickly in both sets of curves; there is a broad peak from approximately 400 to 800 Hz followed by a more or less constant level up to the maximum simulated frequency. In the middle-ear model, there is a clearly defined resonance peak in the vicinity of 1100 Hz that produces an admittance measurement far larger than that seen for the canal wall. Above this frequency, the admittance gradually decreases, reaching a value approximately twice that of the canal wall. Overall, the middle-ear admittance only dominates that of the canal wall in a narrow band around the middle-ear resonance, if at all.

CHAPTER 6: CONCLUSIONS AND FUTURE WORK

6.1 INTRODUCTION

In this chapter, the conclusions that can be drawn from the results of the previous chapter are presented, and potential future work that can be done with these models is discussed.

6.2 CONCLUSIONS

6.2.1 LOW-FREQUENCY SIMULATIONS

In this section of the research, a static model of the newborn ear was used to simulate the response to low-frequency probe-tone input. The simplification of the system to a model where damping and inertia are not included allowed for there to be only one major material property of interest: the Young's modulus. However, this parameter has not been measured experimentally for either the newborn's canal wall or the TM. Therefore, large ranges of possible values were used for their moduli, based on indirect evidence. Within those ranges, parameter values were found such that the models produce an overall behaviour that is in reasonable agreement with measured data. It would be beneficial for future work if the material properties of these newborn tissues were studied more closely so that the parameter choices could be supported by reasonably direct experimental measurements.

The primary justification for using a static simulation is that at low frequencies all of the time-dependent effects become insignificant due to how slowly the system is moving. A reasonable concern about this assumption might be that the frequency at which this simplification is valid is outside of the normal audible hearing range and would not be within the realm of typical tympanometry. However, as seen in Section 5.2.4, the experimental work by Keefe *et al.* (1993) shows that the total compliance of the

ear changes by only 5% as the input frequency is doubled from 125 Hz to 250 Hz. This suggests that the typical 226 Hz probe-tone frequency is low enough, even in newborns, that the displacements of the system are very insensitive to frequency changes and are mostly due to stiffness effects. Therefore, it is reasonable to assume that static simulations are able to give a fairly good estimate of newborn ear behaviour at realistic low probe-tone frequencies.

6.2.2 DYNAMIC SIMULATIONS

The primary goal of tympanometry is the discovery of middle-ear pathologies. It is not needed for analysis of the ear canal since most canal pathologies can be discovered through visual inspection. It is therefore desirable that the admittance signal measured in tympanometry should correspond only to the admittance of the middle ear since this is the only structure of interest. Currently, newborn tympanometry is most often performed at a frequency of 226 Hz for the reasons described in Section 2.8.1. Figure 5.14 shows that at 226 Hz, the canal-wall admittance is as large as or even larger than the middle-ear admittance, so this frequency is far from ideal. In this situation, the signal of interest (middle-ear behaviour) is being combined with an additional signal with minimal clinical value (canal-wall behaviour). It is likely that an important reason for the difficulty in understanding newborn tympanograms is that the canal-wall admittance is mistakenly being interpreted as additional middle-ear admittance.

It is clear that a different probe-tone frequency should be considered for newborn testing, and an obvious choice based on the desired output is in the vicinity of the resonance frequency of the middle ear. At this frequency, the results of this work suggest that the middle-ear admittance is several times larger than the canal-wall admittance. The middle-ear admittance signal would be much larger than the unwanted effect being produced by the canal wall, improving the chance that the data would give useful information about the middle ear. These findings consistent with those of the groups discussed in Section 2.8.2 who have concluded that 1000 Hz is a much better probe-tone frequency to use for newborns.

As seen in Table 5.3, the resonance frequency of the newborn's middle ear is relatively insensitive to parameters such as damping and TM thickness. Therefore, any variation in these parameters, whether they are due to pathology or simply inter-subject variability, will not shift the resonance frequency far away from its typical value. As evidenced by Table 5.3, any significant deviation in the middle-ear resonance frequency is likely due to pathology or anatomical variability affecting the density and/or the Young's modulus of the TM.

The middle-ear admittance resonance peak may be quite sharp, and its position is uncertain. Even a relatively small shift in the location of the peak could be enough to cause large changes in the admittance measured at any one frequency in its vicinity. Because of this, it may be better to measure the admittance at several frequencies in the vicinity of the middle-ear resonance in order to pinpoint its exact location.

As stated in Section 5.3.3, the admittance of the middle-ear model is quite insensitive to any changes to the material properties of the ossicles and their ligaments. This suggests that tympanometry will have difficulty detecting any abnormality or pathology of these structures since they have little effect on the measured admittance.

When using EEM, the perturbations of the parameter values are normalized using a scale defined by the user. In our case, the perturbations were chosen according to the uncertainty present in the experimental measurements. With this choice of scale, it follows that the μ value of a particular parameter will decrease as experimental measurements of its value become more accurate. For example, if the μ value of a parameter is high, this implies that the behaviour of the model will vary widely across the range of potential parameter values, whereas if μ is small, the model will behave similarly regardless of where the parameter magnitude lies within its range of uncertainty. Therefore, parameters with a large μ are the top priority for further study and more accurate measurements. In the case of these models, Table 5.3 seems to suggest that better estimates of the Young's modulus and density are most important for obtaining

more accurate resonance frequencies, while better estimates of the damping ratio and TM thickness are important for obtaining more accurate maximum admittances.

As mentioned in Sections 4.2 and 4.4.2.5, two modelling errors were found after the thesis had been written, examined and passed. First, the anterior-superior quadrant of the TM was set as the thickest rather than the posterior-superior quadrant. Second, the model was elongated in the inferior-superior direction by 25%. Preliminary tests have been done to assess the effects of these errors on the model results.

For the quadrant error, correctly setting the posterior-superior quadrant of the TM as the thickest lowers the maximum admittance of the middle ear by approximately 20%, raises the resonance frequency by approximately 150 Hz, and introduces a secondary peak in the middle-ear frequency response at approximately 900 Hz. For the scaling error, compressing the middle-ear model by 20% in the inferior-superior direction (not changing the already correct TM thickness) lowers the maximum admittance by another 20%; lowers the resonance frequency by approximately 50 Hz; and increases the size of the secondary peak in the frequency-response curve. The changes due to scaling the ear-canal model are much smaller: the resonance frequency only increases by approximately 50 Hz and the maximum admittance only decreases by approximately 7%.

Although the results of these preliminary tests show changes in the results that are not negligible, they are not large compared with the effects of anatomical variability and parameter uncertainty, and the overall conclusions regarding the relative admittances of the ear-canal and middle-ear models remain the same. It appears that the revised models may actually match the experimental data better than the incorrect models do.

6.3 FUTURE WORK

There are several different steps that should be taken to pursue this research. Firstly, there is a need for additional experimental work. Due to a lack of knowledge about the true material properties of the newborn ear, many of the parameter values used

in the models, such as the Young's moduli and damping ratios of the TM and ear canal, were crudely estimated. There is also a need for more precise imaging of the newborn ear. Higher-resolution images would allow for the construction of smoother and more accurate 3-D models and would provide insight into areas such as inter-subject variability and age-related anatomical changes. Overall, the accuracy of the FE simulations is limited by our knowledge of the true system, and therefore further experimental research would be extremely valuable.

A closer look could also be taken at the displacement patterns of the ear canal and the middle ear. In this research, the primary results were the volume displacements and volume velocities of the system. Close attention was not given to results such as the points of maximum displacement, displacements of key points such as the umbo, the spatial distribution of the displacement patterns, etc. Further analysis of these types of simulations results could give valuable insight into the mechanics of the newborn ear canal and middle ear.

Also, the models could be run without assuming that the tympanic ring is fixed in place. This might be a significantly better representation of the actual tympanic ring in newborns (Saunders *et al.* 1983) and would allow the vibrations of the canal wall to affect those of the TM and vice versa. However, this new type of interaction would clearly require that the canal model and middle-ear model be coupled and run simultaneously. This would greatly increase the computation time required.

Another interesting next step would utilize an input pressure that has both a large static component and a small dynamic component, as this is the complete input signal that is used in tympanometry. However, using this type of input would result in several complications. First, the static pressure component of the input can reach up to 4000 Pa, and as shown by Qi *et al.* (2008), this requires a non-linear formulation for the materials in the models. This new type of input pressure would also require that the model solver have extremely high precision. For example, for the case when a 0.4 Pa probe tone is introduced into an ear that is subject to a static pressure of 4000 Pa, the large

displacements caused by the static pressure would be solved with the same tolerance (the allowable error in each integration step) as the much smaller displacements produced by the probe tone. This leads to the necessity for 10000 times less tolerance for the large displacements than would be needed if there was no probe tone. Obviously, a dynamic, non-linear model with a complex geometry and the need for a very high level of precision would require a very powerful computer setup and the simulations would be very time-consuming.

The goal of this work on models of the newborn ear is to be able to accurately simulate the complete response of the newborn ear canal and middle ear to tympanometry. When this is achieved, the results should provide insight into the typical shape of a newborn's tympanogram (see Figure 2.7) and should aid with the proper screening and diagnosis of a newborn's hearing. Additionally, pathological changes, such as a stiffening of the TM or the introduction of fluid in the middle ear, could be introduced into these models. These types of modifications would demonstrate how the newborn tympanogram would differ in these pathological situations and would potentially allow for much greater precision in clinical diagnoses.

APPENDIX

	Young's modulus	Density	Damping Ratio
Baseline	**B**	**B**	**B**
Step 1	+ Δ	B	B
Step 2	+ Δ	+ Δ	B
Step 3	+ Δ	+ Δ	+ Δ
Reset	**B**	**B**	**B**
Step1	B	− Δ	B
Step 2	B	− Δ	− Δ
Step 3	− Δ	− Δ	− Δ
Reset	**+ Δ**	**− Δ**	**+ Δ**
Step 1	+ 2Δ	− Δ	+ Δ
Step 2	+ 2Δ	− 2Δ	+ Δ
Step 3	+ 2Δ	− 2Δ	+ 2Δ

Table A.1 Procedure used for studying the elementary effects of the ear-canal model. B signifies the baseline parameter value at the centre of its range.

	Young's Modulus	Density	Damping Ratio	TM Thickness ¾	TM Thickness ¼	ME Cavity Size
Baseline	**B**	**B**	**B**	**B**	**B**	**B**
Step 1	+ Δ	B	B	B	B	B
Step 2	+ Δ	+ Δ	B	B	B	B
Step 3	+ Δ	+ Δ	+ Δ	B	B	B
Step 4	+ Δ	+ Δ	+ Δ	+ Δ	B	B
Step 5	+ Δ	+ Δ	+ Δ	+ Δ	+ Δ	B
Step 6	+ Δ	+ Δ	+ Δ	+ Δ	+ Δ	+ Δ
Reset	**B**	**B**	**B**	**B**	**B**	**B**
Step 1	B	− Δ	B	B	B	B
Step 2	B	− Δ	B	− Δ	B	B
Step 3	B	− Δ	− Δ	− Δ	B	B
Step 4	B	− Δ	− Δ	− Δ	B	− Δ
Step 5	B	− Δ	− Δ	− Δ	− Δ	− Δ
Step 6	− Δ	− Δ	− Δ	− Δ	− Δ	− Δ
Reset	**+ Δ**	**− Δ**	**+ Δ**	**− Δ**	**+ Δ**	**− Δ**
Step 1	+2Δ	− Δ	+ Δ	− Δ	+ Δ	− Δ
Step 2	+2Δ	− 2Δ	+ Δ	− Δ	+ Δ	− Δ
Step 3	+2Δ	− 2Δ	+2Δ	− Δ	+ Δ	− Δ
Step 4	+2Δ	− 2Δ	+2Δ	− 2Δ	+ Δ	− Δ
Step 5	+2Δ	− 2Δ	+2Δ	− 2Δ	+2Δ	− Δ
Step 6	+2Δ	− 2Δ	+2Δ	− 2Δ	+2Δ	− 2Δ

Table A.2 Procedure used for studying the elementary effects of the middle-ear model. B signifies the baseline parameter value at the centre of its range.

REFERENCES

Alaerts J, Luts H & Wouters J (2007) Evaluation of middle ear function in young children: Clinical guidelines for the use of 226- and 1,000-Hz tympanometry. *Otol & Neurotol* 28: 727–732

Alciatore DG (2007) *Introduction to Mechatronics and Measurement Systems* (3rd ed.). McGraw Hill

Anson BJ, Donaldson JA (1981) *Surgical Anatomy of the Temporal Bone.* Saunders. Pennsylvania

ASHA (1994) Joint Committee on Infant Hearing 1994 Position Statement. *ASHA* 36(12): 38–41

Békésy GV (1960) *Experiments in Hearing*. AIP Press, New York

Bluestone CD, Stool SE (1983) *Pediatric Otolaryngology.* Saunders. Pennsylvania

Cheng T, Dai C, Gan RZ (2007) Viscoelastic properties of human tympanic membrane. *Ann Biomed Eng 35*: 305–314

Cheung JTM, Zhang M, Leung AKL, Fan YB (2004) Three-dimensional finite element analysis of the foot during standing. A material sensitivity study *J Biomech 38*: 1045–1054

Chui C, Kobayashi E, Chen X, Hisada T, Sakuma I (2004) Combined compression and elongation experiments and non-linear modelling of liver tissue for surgical simulation. *Med Biol Eng Comput 42:* 787–798

Decraemer WF, Maes MA, Vanhuyse VJ (1980) An elastic stress–strain relation for soft biological tissues based on a structural model. *J Biomech 13*: 463–468

Decraemer WF, Maes MA, Vanhuyse VJ, Vanpeperstraete P (1980) A non-linear viscoelastic constitutive equation for soft biological tissues, based upon a structural model. *J Biomech* 13: 559–564

Dhar PR, Zu, JW (2007) Design of a resonator device for in vivo measurement of regional tissue viscoelasticity. *Sens and Actu A: Phys* 133: 45–54

Didyk LA, Dirckx JJJ, Bogdanov VB, Lysenco VA, Gorgo YP (2007) The mechanical reaction of the pars flaccida of the eardrum to rapid air pressure oscillations modeling different levels of atmospheric disturbances. *Hearing Research* 223; 20–28

Donaldson JA, Duckert LG, Lambert PM, Rubel EW (1992) *Surgical Anatomy of the Temporal Bone* 4th ed. Raven Press, New York

Funnell WRJ, Laszlo CA (1982) A critical review of experimental observations on eardrum structure and function. *ORL* 44: 181–205

Funnell WRJ (1996) On the low-frequency coupling between eardrum and manubrium in a finite-element model. *J Acoust Soc Am 99*: 3036–3043

Funnell WRJ, Siah TH, McKee MD, Daniel SJ, Decraemer WF (2005) On the coupling between the incus and the stapes in the cat. *JARO* 6(1): 9−18

Fung YC (1993) *Biomechanics: Mechanical Properties of Living Tissues*. second. Springer-Verlag, New York

Ghosh SS (1996) On the effects of incudostapedial joint flexibility in a finite-element model of the cat middle ear. M Eng. Thesis, McGill University, Montreal.

Harkness, RD (1961) Biological functions of collagen. *Biol. Rev. Cambridge Phil. Soc*. 36: 399–463

Hartley JG. (1986) *Fundamentals of the Finite Element Method*. Macmillan. New York

Heneghan P, Riches PE (2008) Determination of the strain-dependent hydraulic permeability of the compressed bovine nucleus pulposus. *J Biomech*. 41:903–6

Holte, L., Margolis, RH. & Cavanaugh, RM. Jr (1991) Developmental changes in multifrequency tympanograms. *Audiology* 30: 1–24.

Holzapfel GA (2000) *Nonlinear Solid Mechanics: A Continuum Approach for Engineering*. Chichester , New York

Hunter, LL. & Margolis, RH. (1992) Multifrequency tympanometry: Current clinical application. *Am J Audiol* 1: 33–43.

James, JF. (2002) *A Student's Guide to Fourier Transforms* (2nd ed.), New York: Cambridge University Press,

Jerger, J. (1970) Clinical experience with impedance audiometry. *Arch. Otolaryngol*. 92, 411–324.

Katz J (2002) *Handbook of clinical audiology*, Lippincott Willams & Wikins

Keefe DH, Bulen JC, Arehart KH, Burns EM (1993) Ear-canal impedance and reflectance coefficient in human infants and adults. *J Acoust Soc Am 94*: 2617–2637

Keefe DH & Levi E (1996) Maturation of the middle and external ears: Acoustic power-based responses and reflectance tympanometry. *Ear & Hearing* 17: 361–373

Kirikae I (1960) *The Structure and Function of the Middle Ear*. University of Tokyo, Tokyo

Klein TJ, Chaudry M, Bae WC, Sah RL (2007) Depth-dependent biomechanical and biochemical properties of fetal, newborn, and tissue-engineered articular cartilage *J Biomech* 40: 182–190

Koike T, Wada H, Kobayashi T (2002) Modeling of the human middle ear using the finite-element method. *J Acoust Soc Am 111*:1306–1317

Kojo Y (1954) Morphological studies on the human tympanic membrane *J.ORL. Soc. Japan* 57: 115–126 (in Japanese).

Kuypers LC, Decraemer WF, Dirckx JJJ (2006) Thickness distribution of fresh and preserved human eardrums measured with confocal microscopy. *Otol Neurotol. 27*: 256–264

Ladak HM (1993) Finite-element modeling of middle-ear prosthesis in cat. M Eng Thesis, McGill University, Montreal.

Lilly D (1984) Multiple frequency, multiple component tympanometry: New approaches to an old diagnostic problem. *Ear Hear 5*: 300–308

Linden G (1969) The scope and application of current audiometric tests. *J. Laryngology Otol*. 83, 507–520.

Liu Y, Kerdok AE, Howe RD (2004) A nonlinear finite element model of soft tissue indentation. Proceedings of Medical Simulation: International Symposium, Cambridge, MA, 67–76

Marazita ML, Ploughman LM, Rawlings B, Remington E, Arnos KS & Nance WE. (1993) Genetic epidemiological studies of early-onset deafness in the U.S. school-age population. *Am J Med Gen* 46: 486–491

Marchant, CD, McMillan, PM, and Shurin, PA (1984) Objective diagnosis of otitis media in early infancy by tympanometry and ipsilateral acoustic reflex thresholds. *J Pediatr* 109: 590–595.

Margolis RH & Popelka GR (1975) Static and dynamic acoustic impedance measurements in infant ears. *J Speech Hear Res* 18: 435–443

Margolis RH, Bass-Ringdahl S, Hanks WD, Holte K & Zapala DA (2003) Tympanometry in newborn infants – 1 kHz norms. *J Am Acad Audiol* 14: 383–392

McGarry MD, Van Houten EE (2008) Use of a Rayleigh damping model in elastography. *Med Biol Eng Comput.* 46: 759–766

McLellan MS & Webb CH (1957) Ear studies in the newborn infant: natural appearance and incidence of obscuring by vernix, cleansing of vernix, and description of drum and canal after cleansing. *J Pediatr* 51: 672–677

Meyer SE, Jardine CA & Deverson W (1997) Developmental changes in tympanometry: A case study. *Brit J Audiol* 31: 189–195

Molvaer O, Vallersnes F, Kringlebotn M (1978) The size of the middle ear and the mastoid air cell. *Acta Oto-Laryngol. 85*: 24–32

NIDCD (1993) National Institutes of Health Consensus Statement: Early identification of hearing impairment in infants and young children. National Institute on Deafness and Other Communication Disorders, Bethesda, MD

Paradise JL, Smith CG & Bluestone CD (1976) Tympanometric detection of middle ear effusion in infants and young children. *Pediatrics* 58: 198–210.

Qi L, Liu H, Lutfy J, Funnell WRJ & Daniel SJ (2006) A non-linear finite-element model of the newborn ear canal. *J Acoust Soc Am* 120: 3789–3798

Qi L, Funnell WRJ & Daniel SJ (2008) A non-linear finite-element model of the newborn middle ear. *J Acoust Soc Am* 124: 337–347

Qi L (2008) Non-linear finite-element modeling of newborn ear canal and middle ear. Ph.D. Thesis, McGill University, Montreal

Ruah CB, Schachern PA, Zelterman D, Paparella MM, Yoon TH (1991) Age-related morphologic changes in the human tympanic membrane. A light and electron microscopic study. *Arch Otolaryngol Head Neck Surg. 117*: 627–634

Saltelli, A, Tarantola S, Campolongo F & Ratto M (2004) *Sensitivity Analysis in Practice: A Guide to Assessing Scientific Models*. Chichester: Wiley

Saunders JC, Kaltenbach JA, Relkin, EM (1983) The structural and functional development of the outer and middle ear. In R. Romand (Ed). *Development of Auditory and Vestibular Systems*. New York: Academic

Shanks JE, Lilly DJ (1981) An evaluation of tympanometric estimates of ear canal volume. *J Speech Hear Res 24*: 557–566

Shurin PA, Pelton SI & Finkelstein J (1977) Tympanometry in the diagnosis of middle-ear effusion. *N Engl J Med* 296: 412–7.

Siah TS (2002) Finite-element modeling of the mechanics of the coupling between the incus and stapes in the middle ear. M Eng. Thesis, McGill University, Montreal.

Steele DG, Bramblett CA (1988) The Anatomy and Biology of the Human Skeleton. Texas A&M University Press. p. 4.

Stepp CE, Voss SE (2005) Acoustics of the human middle-ear air space. *J Acoust Soc Am. 118(2)*: 861–871

Stinson MR, Lawton BW (1989) Specification of the geometry of the human ear canal for the prediction of sound-pressure level distribution. *J Acoust Soc Am 85*: 2492–503

Watters GWR, Jones JE & Freeland AP (1997) The predictive value of tympanometry in the diagnosis of middle ear effusion. *Clin Otolaryngol* 22: 343–345

Wellman P, Howe RH, Dalton E, & Kern KA (1999) Breast tissue stiffness in compression is correlated to histological diagnosis. Technical report, Harvard Biorobotics Laboratory, http://biorobotics.harvard.edu/pubs/mechprops.pdf

Widmaier EP, Raff H, Strang KT (2006) *Vander's Human Physiology, The Mechanisms of Body Function*. McGraw Hill, New York

Williamson AK, Chen AC, Sah RL (2001) Compressive properties and function-composition relationships of developing bovine articular cartilage. *J Orthop Res 19*: 1113–1121

Zhang M, Zheng YP, Mak AF (1997) Estimating the Effective Young's Modulus of Soft Tissues from Indentation Tests – Nonlinear Finite Element Analysis of Effects of Friction and Large Deformation. *Med Eng Phys 19*: 512–517

Zwislocki J (1962) Analysis of the middle-ear function. 1. Input impedance. *J Acoust. Soc. Am. 34*: 1514–1523